Colloquium: Room temperature superconductivity: The roles of theory and materials design

Warren E. Pickett⬤

Department of Physics and Astronomy, University of California, Davis,
Davis, California 95616, USA

(published 7 April 2023)

For half a century after the discovery of superconductivity, materials exploration for better superconductors proceeded without knowledge of the underlying mechanism. The 1957 BCS theory cleared that up. The superconducting state occurs due to strong correlation in the electronic system: pairing of electrons over the Fermi surface. Over the following half century a higher critical temperature T_c was achieved only serendipitously as new materials were synthesized. Meanwhile, the formal theory of phonon-coupled superconductivity at the material-dependent level became progressively more highly developed: by 2000, given a known compound, its value of T_c, the corresponding superconducting gap function, and several other properties of the superconducting state became available independent of further experimental input. In this century, density-functional-theory-based computational materials design has progressed to a predictive level; new materials can be predicted from free energy functionals on the basis of various numerical algorithms. Taken together these capabilities enable theoretical predictions for new superconductors, justified by applications to superconductors ranging from weak to strong coupling. Limitations of the current procedures are discussed; most of them can be handled with additional procedures. Here the process that has resulted in the three new highest temperature superconductors is recounted, with compressed structures predicted computationally and values of T_c obtained numerically that have subsequently been confirmed experimentally: the designed superconductors SH_3, LaH_{10}, and YH_9. These hydrides have T_c in the 200–260 K range at megabar pressures; the experimental results and confirmations are discussed. While the small mass of hydrogen provides the anticipated strong coupling at high frequency, it is shown that it also enables identification of the atom-specific contributions to coupling, in a manner that was previously possible only for elemental superconductors. The following challenge is posed: that progress in understanding of higher T_c is limited by the lack of understanding of screening of H displacements. Ongoing activities are mentioned and current challenges are suggested, together with regularities that are observed in compressed hydrides that may be useful to guide further exploration.

CONTENTS

I. INTRODUCTION

Room temperature superconductivity (RTS) has been one of the grand challenges of condensed matter physics since the BCS theory of pairing (see Sec. II.A) was proposed and its predictions verified. The distinctive electronic and magnetic properties of the superconducting state readily suggest copious applications, both in the laboratory and in the public sector. The slow progress in increasing the maximum critical temperature T_c from 4 K in 1911 to 23 K in 1973 (3 K/decade), followed by a 15 year plateau, moved this imposing challenge well into the background. The discovery of high T_c cuprates [up to 134 K, or 164 K under pressure (Gao *et al.*, 1994)] involving magnetic interactions introduced a new type of superconductivity (SC) and generated renewed interest. After eight years of advancement of T_c, another plateau in cuprate superconducting T_c has thus far lasted for 28 years. This recent advancement of the maximum T_c, revealing a breakthrough increase toward room temperature superconductivity that prompted this Colloquium, is shown in the upper right corner of Fig. 1. After preliminary information, in Secs. V and VI these advancements and some of their microscopic origins are discussed.

Much attention has centered on guidelines ("rules," or "road maps") necessary for high T_c, thereby presumably pointing the way to yet higher T_c. Such rules have been based primarily on known superconductors and have subsequently been set aside as entirely new classes of superconductors were discovered, almost entirely by serendipity. In the 1960s empirical trends led to "Matthias's rules." These stated that for high T_c one should search for (1) cubic materials, (2) d electrons at the Fermi level, and (3) specific electron-to-atom ratios. The third rule was soon understood to mean a high density of electron states at the Fermi level ($\varepsilon_F = 0$) $N(0)$, i.e., a high density of superconducting pairs. Matthias's group had been the leader in the discovery of new superconductors in the 1950s and early 1960s, after which the search extended worldwide.

Though unwritten, additional rules were advertised: (4) stay away from oxygen, which produces unpredictable behavior including insulation, and (5) stay away from magnetism, which at the time competed too strongly with superconducting pairing. Matthias had an additional personal rule: (6) stay away from theorists, as they are of no help. [Matthias did write, without elaboration, "I never realized how many of my friends are theorists" (Matthias, 1972).] The last rule was based on his observation that knowing the theory of SC, at least in a broad model BCS way, had been useless in helping discovery; what worked was simply to "follow the simple road map." However, the rules did not produce high T_c materials.
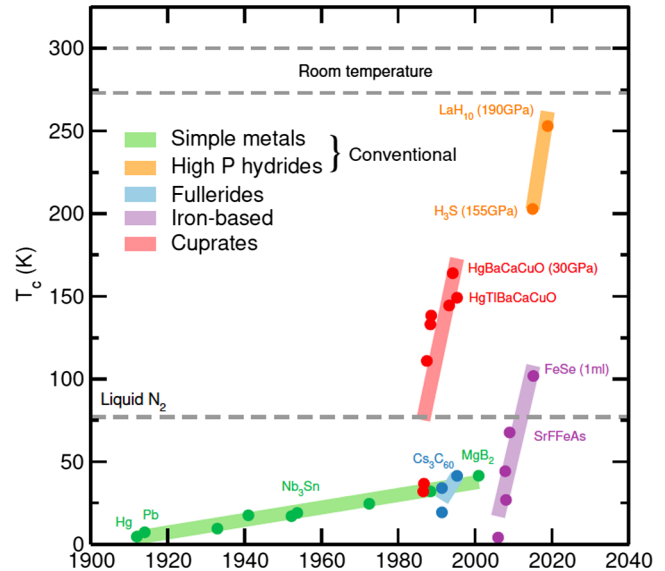
FIG. 1. Plot of the major advances in the maximum T_c vs year from the discovery of superconductivity in Hg in 1911 and using linear scales. Advances within classes are denoted by thick linear areas, with color delineating different classes. Certain temperature hurdles are denoted by dotted horizontal lines. High-pressure hydrides lie at the upper right (yellow), with temperatures converging toward room temperature. From Pickett and Eremets, 2019.

It continued to be true through cuprate days (after the initial high T_c) that theory played no part in the advance of the maximum T_c from 4 K in Hg to 134 K in cuprates.

Over the intervening decades theory and numerical implementation have advanced. While overt activity toward higher BCS superconductivity has waned, intellectual interest in the goal of RTS has persisted, with evidence given by various international workshops indicating continued emphasis on room temperature explorations.[1] With the 2014–2015 discovery of extreme high T_c SC in compressed metal hydrides under pressure discussed in this Colloquium, the roles of experiment and theory evolved and were reversed. Theory has assumed a prominent role as predictor beyond the maximum known T_c (T_c^{max}) for phonon-coupled SCs as they jumped from 40 to 200 K, then rapidly marched toward room temperature.

After recounting the sequence of necessary theoretical advances in Sec. II, we give in Sec. III an indication of the computational innovation and implementations that were required to design real, heretofore unknown materials. An

---

[1]Six of the meetings follow: The Road to Room Temperature Superconductivity, Bodega Bay, California, 1992; The Possibility of Room Temperature Superconductivity, University of Notre Dame, June 10 and 11, 2005 (https://www3.nd.edu/~its/rts/index.html); (Toward) Room Temperature Superconductivity, Leiden, Netherlands, 2014; SUPERHYDRIDES: Towards Room Temperature Superconductivity: Hydrides and More, Rome, Italy, 2016; Towards Room Temperature Superconductivity: Superhydrides and More, Chapman College, California, 2017; and Challenges in Designing Room Temperature Superconductors, L'Aquila, Italy, 2022.

overview of the rising research area in this century of crystal structure prediction is given in Sec. IV. Section V provides a description of the first three revolutionary discoveries of critical temperatures in the 200–260 K range. Thus far these (and a few others) have all required megabar pressures. The discussion in Sec. VI reveals how the light H atom restores the sort of analysis that was developed for elemental metals, which leads to a demonstration that H dominates the metal component in promoting high T_c. In fact, the contribution of the metal atom provides confusion by contributing in opposing ways to the properties that promote high T_c. This leads to Sec. VI, which gives an overview of near-term challenges and opportunities that have been identified in the high T_c arena. These are provided in terms of several regularities of high T_c compressed hydrides that may guide the next level of searches, as compiled in Sec. VII. Section VIII provides conclusions.

II. THEORETICAL DEVELOPMENTS THROUGH THE DECADES

The impetus for this noteworthy breakthrough has been a sequence of advances in theory, numerical implementation, and computational design together with mastery of high-pressure techniques. Since this advance in computational theory has extended over six decades (i.e., three generations of physicists), we provide in this section an overview of the fertile path of breakthroughs in theory and numerical implementation that have enabled current capabilities and their paradigm-revising results.

A. BCS theory

In 1957 Bardeen, Cooper, and Schrieffer published their 30-page magnum opus "Theory of superconductivity" (Bardeen, Cooper, and Schrieffer, 1957), which includes approximately 275 numbered equations. This theory introduced a correlated many-body wave function based on a Fermi surface pairing of electrons demonstrated a year earlier by Cooper. This wave function described a thermodynamic condensate of correlated pairs below a critical temperature T_c, assuming an attractive effective pairing potential arising from exchange of phonons and screened electron-electron scattering. The primary result of their theory was the T_c equation (units $\hbar = 1$ and $k_B = 1$ are used in this Colloquium)

$$T_c^{\text{BCS}} = 1.14\,\Omega\,e^{-1/\lambda^*}, \tag{1}$$

where Ω is the characteristic phonon frequency. $\lambda^* = N(0)V = \lambda - \mu^*$ in terms of terminology developed later (discussed in the following). The Fermi level density of states $N(0)$ is a measure of the density of electrons interacting through the phenomenological coupling V, which BCS noted is the *net interaction* of phonon attraction plus Coulomb repulsion.

The electron-phonon coupling strength λ is the measure of the attractive pair coupling strength by exchange of phonons. Out of interest for the following content of this Colloquium we note that the strong-coupling limit $\lambda^* \to \infty$ leads in this
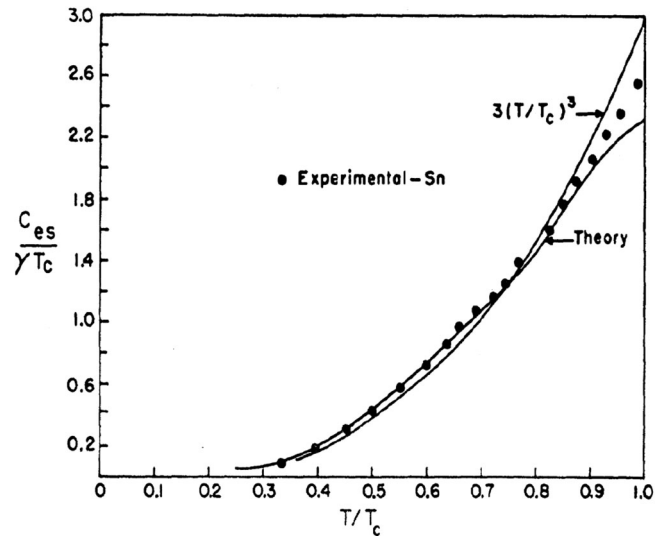
FIG. 2. Illustration of the predicted temperature dependence of the ratio of the specific heat in the superconducting state to that in the normal state value (equal to 1.0 on the abscissa). The behavior is exponentially small at low temperature due to the energy gap, which is in good agreement with experimental data. From Bardeen, Cooper, and Schrieffer, 1957.

expression to a maximum SC temperature of 1.14 Ω, which can be well above room temperature. The theory is, however, valid only for weak coupling, leaving open the question of high T_c and the large λ regime. "High T_c" would be confronted only three decades later with the discovery of cuprate superconductors, for which there is no predictive theory and hereafter is not considered.

The second property of note, provided by BCS theory and its extensions, is the superconducting gap $[\Delta(\omega, T)]$ equation that gives T_c when linearized ($\Delta \to 0$) and at finite temperature provides the frequency ω and temperature T dependence of the energy gap that is responsible for many of the interesting properties of superconductors. The novelty is that a perfect conductor can have a gap for excitations. This gap leads to a vanishing magnetic susceptibility in its interior. It is a basic player in zero resistivity, and it severely alters the thermodynamic, optical, and transport properties.

The effect on the electronic specific heat, shown in Fig. 2, is to make it vanish exponentially as $T \to 0$ rather than linearly to 0 as for the normal metal. The theory was soon generalized by Gor'kov (1958), who used thermodynamic field theory to derive the much used 1950 phenomenological free energy theory of Ginzburg and Landau (1950). This extension of theory also provided a direction for pursuing necessary developments, especially a microscopic understanding of total electron-electron interactions in metals, a path that is discussed later.

B. Migdal-Eliashberg theory

The microscopic Migdal-Eliashberg theory of 1960 (henceforward called Eliashberg theory) of electron-phonon (EP) coupled superconductivity, weak or strong, followed quickly after the model BCS theory (1957) based on a model pairing Hamiltonian and a variational treatment. Recall that the full,

exact (nonrelativistic) Hamiltonian $\mathcal{H}$ for a system of ions $\{\vec{R}\}$ and electrons $\{\vec{r}\}$ is given by

$$\mathcal{H} = [\mathcal{T}^{\text{el}}(\{\vec{r}\}) + \mathcal{V}^{\text{el-el}}(\{\vec{r}\})] + \mathcal{V}^{\text{el-ion}}(\{\vec{r}\}, \{\vec{R}\})$$
$$+ \mathcal{T}^{\text{ion}}(\{\vec{R}\}) + \mathcal{V}^{\text{ion-ion}}(\{\vec{R}\}) \qquad (2)$$

in terms of the various kinetic $\mathcal{T}$ and potential $\mathcal{V}$ energies. The middle term contains the bare electron-ion interaction. With roughly 10^{20} dynamical coordinates per mm^3, this all-encompassing operator is the fundamental, intractable feature of materials theory that requires innovative approaches and reliable approximations.

Migdal (1958) formalized the observation that the great differences in energy scales (or velocities, or masses) of electrons and ions leads to negligible contributions beyond second-order perturbation theory in EP scattering. Eliashberg made the formidable step of placing the pairing theory within the newly developed many-body theory (the thermal Green's function) that made it applicable to the superconducting state (Eliashberg, 1960, 1961), leaving generalizations to materials with crystal structure and lattice effects as a later step (discussed in the following). This Eliashberg formalism provided the fundamental equations for calculating the gap function (superconducting order parameter), given the Eliashberg spectral function $\alpha^2 F(\omega)$ defined in Sec. II.E that provides the essential input for the pairing process. Calculation of this function necessitated several theoretical and algorithmic advances.

C. Density functional theory (DFT)

Hohenberg, Kohn, and Sham followed immediately (1965–1967) with density functional theory (Hohenberg and Kohn, 1964; Kohn and Sham, 1965), which makes the full crystalline Hamiltonian in Eq. (2) treatable (for static nuclei) for many properties of materials for electrons in their ground state, given a reasonable approximation of many-body effects (through an exchange and correlation functional). (The many following extensions of DFT to other properties are not relevant here, except as noted.)

An extremely important aspect of DFT is that it provides a highly reliable one-electron ("mean-field") set of Kohn-Sham one-electron band energies and wave functions (Kohn and Sham, 1965) for use in themselves, and also for applications in treating dynamic behavior that is averaged over in DFT. This DFT breakthrough accelerated activity in band theory, which had already been in progress since the late 1930s based on more phenomenological grounds. The late 1970s saw the accomplishment of achieving self-consistent electronic charge densities, bands, and wave functions. Many applications of electronic ground state energies were explored in the 1980s and afterward.

Calculation of energies for any configuration of atoms enabled the evaluation of interatomic force constants between displaced atoms, and thereby phonon spectra. Initially this was accomplished for each phonon independently, but capabilities were rapidly extended, especially by applying density functional perturbation theory and Wannier function techniques (Rabe and Wagmare, 1995; Cockayne, 2005;

Mostofia *et al.*, 2008). The outcome was true harmonic phonon frequencies through formalism making use of infinitesimal atomic displacements. The change in the electronic potential due to an atomic displacement is also the root factor in EP coupling, and calculation of EP matrix elements was achieved only around 2000.

D. Extension of Eliashberg theory to real materials

In the mid-1960s, the challenge of addressing real superconductors versus simplified models, a prerequisite for materials design and discovery, was accomplished by Scalapino *et al.* in 1964 (Scalapino, Schrieffer, and Wilkins, 1966; Scalapino, 1969). Starting with the full Hamiltonian of a solid (2), they derived a complete formalism for the superconducting Green's function and the full frequency and temperature dependence of the complex gap function. Their formalism awaited a viable description of the underlying electronic energy bands and phonon frequencies and their coupling. The DFT capabilities discussed in Sec. II.C would provide the underlying electronic bands and wave functions, phonon dispersion curves and polarizations, and EP matrix elements.

The validity of their formalism, which underlies today's numerical implementation, relies on a few approximations. First is Migdal's previously mentioned theorem: the vast differences in masses of electrons and ions (more precisely, differences in the frequencies of their dynamic responses) specify that second-order perturbation theory is sufficient for the electron and phonon self-energies. Second is that electron-electron Coulomb repulsion effects leave the metal as a conventional Fermi liquid; specifically, the possibility of magnetic order and magnetic fluctuations is not included at the level that we discuss here.

Third is that the symmetry broken at the superconducting phase transition is the so-called gauge symmetry; in picturesque language, two electrons can form a Cooper pair and disappear into the condensate, or the inverse process can happen. In this language, electron number conservation is broken. C. N. Yang emphasized that electrons do not actually disappear, and that the fundamental signature of the superconducting state is the appearance of long-range order in the two-particle density matrix (Yang, 1962). Finally, for EP-coupled superconductors it is nearly always the case that the superconducting order parameter is proportional to the gap function, i.e., a complex scalar and not a vector or tensor quantity, and other symmetries are not broken at T_c. The resulting theory has passed numerous tests as being accurate for EP-coupled superconductors.

E. Analysis of T_c and discussion of a maximum

1. McMillan's analysis

In 1967 McMillan substantially advanced the analysis of the origins of T_c (McMillan, 1968). He defined the electron-phonon spectral function $\alpha^2 F$, also called the Eliashberg function, in terms of the various quantities appearing in the following Scalapino, Schrieffer, and Wilkins (1966) expresssion:

$$\alpha^2 F(\omega) = N_\uparrow(0) \frac{\sum_{kk'} |M_{kk'}|^2 \delta(\omega - \omega_{k-k'}) \delta(\varepsilon_k) \delta(\varepsilon_{k'})}{\sum_{kk'} \delta(\varepsilon_k) \delta(\varepsilon_{k'})}, \quad (3)$$

where the Fermi energy $\varepsilon_F = 0$ and $k - k'$ is the wave vector of the phonon scattering an electron from state k to k', each confined to the Fermi surface. The necessary sums over bands and phonon branches are not explicitly displayed. The sums that are shown are each over the three-dimensional Brillouin zone, each confined by the pair of δ functions to the Fermi surface. The frequency δ function provides the frequency resolution of coupling. For clarity, the density of states factor is for a single spin, designated as the arrow in $N_\uparrow(0)$.

The EP coupling strength λ and the two frequency moments $\omega_{\log}$ and ω_2 used prominently by Allen and Dynes (1975) (see Sec. II.E.2) are given in terms of moments of 2 $\alpha^2 F(\omega)/\omega$ by

$$\lambda = \int d\omega \frac{2\alpha^2 F(\omega)}{\omega}, \quad (4)$$

$$\omega_2^2 = \int d\omega \omega^2 \frac{2}{\lambda} \frac{\alpha^2 F(\omega)}{\omega} = \int d\omega \omega^2 g(\omega), \quad (5)$$

$$\omega_{\log} = \exp\left[\int d\omega \log \omega g(\omega)\right]. \quad (6)$$

In Eqs. (5) and (6) $g(\omega)$, defined in Eq. (5), is the normalized shape function of $\alpha^2 F(\omega)/\omega$. Aside from normalization, these are all different moments of 2 $\alpha^2 F(\omega)/\omega$. The calculation of $\alpha^2 F$, which is necessary for the computational program to advance, is further discussed in Sec. III.B.

For elemental metals, McMillan initially obtained two fundamental expressions from $\alpha^2 F$. The first is that its first frequency moment is independent of vibrational properties aside from an overall inverse mass factor:

$$\int \omega \alpha^2 F(\omega) d\omega = \frac{N(0)\mathcal{I}^2}{2M}, \quad (7)$$

where $\mathcal{I}^2$ is the average atomic scattering strength by phonons from the Fermi surface to the Fermi surface:

$$I_{k,k'} = \langle k| \frac{dV(r; \{R\})}{dR_j} |k'\rangle,$$

$$M_{k,k'} = \sqrt{\frac{\hbar}{2M\omega_{k-k'}}} I_{k,k'},$$

$$\mathcal{I}^2 = \langle |I_{k,k'}|^2 \rangle_{\text{FS}}. \quad (8)$$

In Eq. (8) $V(r; \{R\})$ is the total electronic potential that depends on all ionic coordinates $\{R\}$, R_j is the coordinate of the displaced atom under consideration, and $I_{k,k'}$ is the electron-ion matrix element between electron states k and k'. $M_{k,k'}$ is the electron-phonon matrix element that contains the atom mass M and phonon frequency $\omega_{k-k'}$, and the outside brackets indicate that an average is taken over all k and k' (both on the Fermi surface) to obtain $\mathcal{I}^2$. This first-order change in potential dV/dR has a long history (Pickett, 1979) and has shown much progress in numerical evaluation,

without much progress in understanding. This integral expression holds only for elements with mass M, a restriction we manage to relax for hydrides in Sec. VII.B.

McMillan's second observation was that (again for elemental metals) λ can be expressed simply in terms of physical quantities,

$$\lambda = \frac{N(0)\mathcal{I}^2}{M\omega_2^2} \equiv \frac{\eta}{\kappa}. \quad (9)$$

The numerator $\eta = N(0)\mathcal{I}^2$ in Eq. (9) is the McMillan-Hopfield factor that reflects an "electronic stiffness," divided by $\kappa = M\omega_2^2$, which is the standard harmonic oscillator form of lattice stiffness (mean force constant), with ω_2 representing the entire spectrum of frequencies. All are normal state properties. Equation (9) indicates that increasing the frequency scale ω_2, which helps T_c, will decrease λ according to its square, thereby hurting T_c, with the net outcome yet to be understood.

As an aside, the simple expression (9) does not apply to compounds, as the quantities $N(0)$ and ω_2 have contributions from all atoms, and $\mathcal{I}^2$ and M are distinct atomic quantities. It is seen in Sec. VI.B that this simple "elemental" expression for λ can be extended to compressed metal hydrides to obtain these quantities separately for H and the metal atom, thereby allowing a deeper analysis into the origins of high T_c.

Most prominently McMillan (1968) provided, with a justification for chosen algebraic forms, a seminal analysis from Eliashberg theory of T_c and its dependence on $\alpha^2 F(\omega)$, presenting his iconic "McMillan equation" expressing T_c via two materials quantities, the phonon Debye frequency θ and λ. A phenomenological retarded Coulomb repulsion $\mu^* = 0.13$ was included in the Eliashberg equation that was solved to relate T_c to $\alpha^2 F$. Solutions for various $\alpha^2 F$ functions were fit to a generalization of the BCS equation of the form

$$T_c^{\text{McM}} = \frac{\theta}{1.45} \exp\left[-1.04 \frac{1 + \lambda}{\lambda - \mu^* - 0.62\lambda\mu^*}\right]$$
$$\equiv \frac{\theta}{1.45} \exp\left(-\frac{1 + \lambda}{\lambda - \mu_{\text{eff}}^*}\right)^{1.04}, \quad (10)$$

where the second expression emphasizes the generalization of the BCS relation. The constants provided best fits to the computational data: the exponent 1.04 seems to be a parameter giving the best fit without any physical significance. Note that the McMillan equation is not appropriate for significantly weak coupling; when the denominator of the argument of the exp function becomes negative, the result is nonsensical. What the McMillan equation does is to replace the involved functional dependence $T_c(\alpha^2 F, \mu^*)$ with a simple equation for T_c involving two quantities from $\alpha^2 F$ plus μ^*.

The effective Coulomb repulsion $\mu_{\text{eff}}^* = \mu^*(1 + 0.62\lambda)$ is defined here (without physical justification) to emphasize the similarity to the BCS equation (1). The $1 + \lambda$ factor in the numerator is often assigned to the strong-coupling electron mass renormalization by EP coupling. The precise extent to which McMillan's $1 + \lambda$ factor, when removed from the experimental specific heat coefficient, produces agreement with the "bare" band theory value of $N(0)$ for 5d alloys is presented in Fig. 3. The mass enhancement is well known to
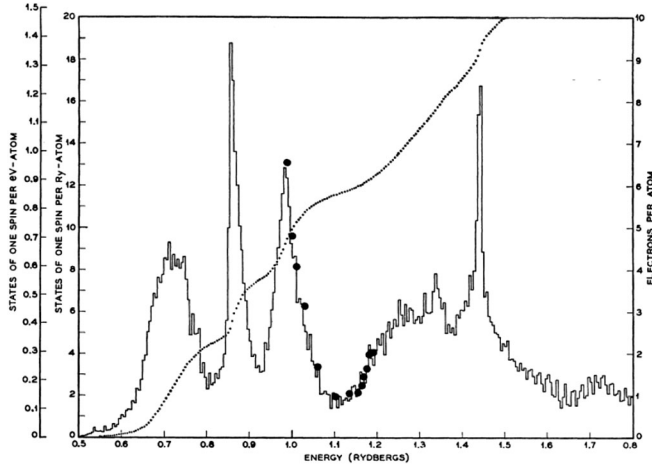
FIG. 3. McMillan's plot for $5d$ transition metal alloys, of the experimental values (dots) of the band structure Fermi level densities of states, for which the mass enhancement $1 + \lambda$ of the specific heat constant γ has been removed, compared to the band theory calculation of tungsten by L. F. Matthiess. The agreement is noteworthy. From McMillan, 1968.

increase the density of active states at the Fermi level by $1 + \lambda$, but in this expression the effect in the numerator is to decrease T_c, compensated somewhat by the $\lambda\mu^*$ term in the denominator. Flores-Livas *et al.* (2020) reproduced the model, which gives a similar result for $\mu^*(\lambda = 0)$ and a different expression for the prefactor.

In McMillan's time the experimental Debye frequency θ for elemental metals was the most accessible measure of the frequency spectrum; however, McMillan recognized that using moments from $\alpha^2 F$ (such as the second moment ω_2) would be more representative.

Only values of λ to around unity were included in McMillan's fit. An extrapolation of T_c^{McM} shows that it saturates for large λ; however, the equation is justified only for moderately strongly coupled superconductors. The limited range of input ($\lambda < 1$) is frequently missed or forgotten and, prior to the discoveries discussed in Secs. II.E.2 and II.E.3, one could still find statements in the literature and in presentations that theory shows that the maximum T_c is limited, perhaps to around 40 K. This point is clarified later.

2. Bergmann and Rainer's functional derivative

In 1973 Bergmann and Rainer (Bergmann and Rainer, 1973) raised a straightforward issue: to increase T_c, one needs to understand the effect on T_c due to an added increment of coupling $\Delta\alpha^2 F(\omega)$ at frequency ω. It seemed clear from the BCS equation that adding coupling at high frequency, seemingly increasing both ω (or Ω or θ, depending on the treatment of the phonon system) and λ (adding an increment), would raise T_c. Soon after McMillan Allen (1973, 1974) gave suggestions that, due to this complex interdependence of materials properties, including $N(0)$ and $\mathcal{I}^2$, coupling at low frequency might even be harmful for T_c. We will see in Sec. VI.B that compressed hydrides provide an unexpected field of study of this unsettled problem.

Bergmann and Rainer addressed the issue by calculating the differential quantity in the kernel of
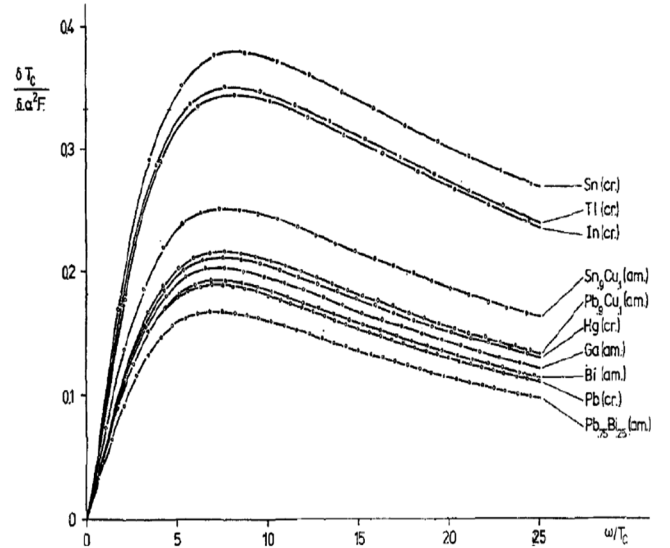

FIG. 4. Bergmann and Rainer's plots of $\delta T_c / \delta\alpha^2 F(\omega)$ vs the ratio ω/T_c for a number of superconductors (as labeled). Its value peaks near $\omega = 2\pi T_c$ and decreases slowly thereafter, indicating little importance of low energy phonons and great importance for higher energies. From Bergmann and Rainer, 1973.

$$\Delta T_c = \int d\omega \, \frac{\delta T_c[\alpha^2 F, \mu^*]}{\delta\alpha^2 F(\omega)} \Delta\alpha^2 F(\omega), \qquad (11)$$

which is the functional derivative of T_c with respect to $\alpha^2 F(\omega)$. Given an increase in coupling by an increment $\Delta\alpha^2 F$ at frequency ω, what is the change ΔT_c?

They established that this functional derivative is smooth ($\alpha^2 F$ is not) and non-negative; thus every phonon helps, as anticipated. At least for conventional shapes and strengths of $\alpha^2 F$, it has a broad peak around $\omega_{\mathrm{BR}} \sim 2\pi T_c$ followed by a slow decrease at high frequency (shown in Fig. 4). Conversely, below ω_{BR} the usefulness of coupling decreases linearly to zero. Low frequencies can and do contribute strongly to λ: viz., the corresponding functional derivative is $\delta\lambda / \delta\alpha^2 F(\omega) = 2/\omega$.

This result, viz., that coupling at high frequencies is most important, does not resolve all issues. While adding some differential coupling $\Delta\alpha^2 F(\omega)$ does affect both λ and ω calculated from $\alpha^2 F$, in the larger picture it also will affect the EP coupling that causes changes in $\alpha^2 F$ at frequencies besides ω. This effect is not settled by simply including a single extrinsic increment in $\alpha^2 F$. It is seen in Sec. VI.B that hydrides provide counterexamples to the simple interpretation offered by the functional derivative of Bergmann and Rainer.

3. Allen and Dynes's reanalysis

Building on the work of McMillan, Allen and Dynes in 1975 presented a reanalysis (Allen and Dynes, 1975) of T_c, using more than 200 solutions of the Eliashberg equation for λ up to 10 and μ^* up to 0.20, including experimental determinations of $\alpha^2 F$ (by numerical inversions of tunneling data) with associated measured T_c. Allen and Dynes chose to generalize the McMillan equation. Most obvious is that the frequency prefactor is updated from ω_2 (altered earlier from
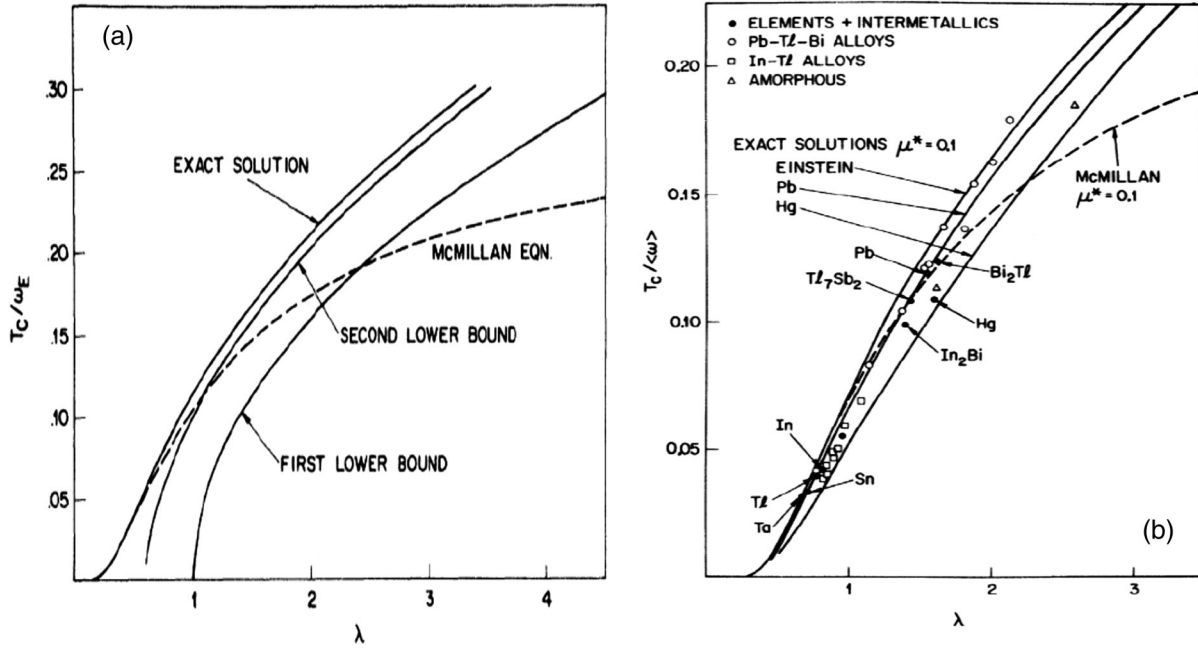
FIG. 5. (a) Allen and Dynes's plots of the ratio $T_c/\langle\omega\rangle$ vs λ for the McMillan equation, and for truncated and exact numerical results from the Eliashberg equation. (b) Similar plots using data for several known strong coupled superconductors. Also shown is the exact solution for an Einstein model with frequency $\langle\omega\rangle = \Omega$, with the deviation from the McMillan equation beginning at $\lambda \sim 1$. Here $\langle\omega\rangle$ is the conventional first moment of $\alpha^2 F(\omega)/\omega$. From Allen and Dynes, 1975.

McMillan's θ) to the logarithmic moment $\omega_{\log}$ with an adjusted constant, as the latter produced a more consistent fit to their data.

More importantly, they observed that corrections were needed both for the strength of coupling (they considered much larger values of λ than were previously studied) and for unusual shapes of the $\alpha^2 F/\omega$ spectrum. For example, the textbook shape of the Nb phonon spectrum is much different from that of, say, PdH, which consists of low frequency Pd acoustic modes separated from high frequency H optic modes. We return to the implications of this two-peak shape in Sec. VI.B.

The shape dependence was framed by Allen and Dynes in terms of the ratio $\omega_2/\omega_{\log}$, which is always greater than unity. In their fit to extensive data, the argument of the exponent was not changed; rather, each change (strong coupling and shape) was incorporated into its own prefactors f_1 and f_2, respectively. The Allen-Dynes equation can be written, considering the previously given McMillan form,

$$
\begin{aligned}
T_c^{\mathrm{AD}} &= \frac{\omega_{\log}}{1.20}\frac{1.45}{\theta}f_1(\lambda,\mu^*)f_2(\omega_{\log},\omega_2)T_c^{\mathrm{McM}}(\lambda,\mu^*)\\
&= \frac{\omega_{\log}}{1.20}f_1 f_2 \exp\left(-\frac{1+\lambda}{\lambda-\mu_{\mathrm{eff}}^*}\right)^{1.04}\\
&= \frac{\omega_{\log}}{1.20}f_1 f_2 \exp\left[-1.04\frac{1+\lambda}{\lambda-\mu^*-0.62\lambda\mu^*}\right],
\end{aligned}
\tag{12}
$$

with the latter form the more common one and the one presented by Allen and Dynes. The simple expressions for f_1 and f_2 can be found in the original paper (Allen and Dynes, 1975). Note that θ cancels in the first expression and is replaced by the logarithmic frequency moment, which Allen

and Dynes found to be the most useful moment for the prefactor of T_c.

Owing to the f_1 and f_2 factors, T_c^{AD} is no longer exponential in the argument involving λ except in the weak-coupling region, where λ begins to approach μ^*. In this regime a solution of the Eliashberg equation, as well as T_c^{AD}, is highly sensitive to each quantity. For this reason, their equation is not a meaningful fit to any data in this weak-coupling region. For the high T_c compressed hydrides discussed in Sec. V, each prefactor can approach a 10%–20% enhancement of T_c (or increasingly more as λ is further increased).

A crucial finding of Allen and Dynes was that in the large λ regime, where analytic results could be extracted, the asymptotic behavior is

$$
T_c \to 0.18\sqrt{\lambda\omega_2^2} = 0.18\omega_2\sqrt{\lambda} = 0.18\sqrt{\eta/M}
\tag{13}
$$

for $\mu^* = 0.10$ (the prefactor depends somewhat on μ^*). In Eq. (13) $\lambda = \eta/M\omega_2^2$ for elements has been used to display different viewpoints. Note that the asymptotic limit involves only the same frequency-independent constant identified by McMillan in Eq. (7). A primary implication is that Eliashberg theory poses no limit on T_c. Figure 5(a) shows some of the numerical data that establishes the ever-increasing (not plateauing) of $T_c(\lambda)$, and Fig. 5(b) provides numerical data using experimental shapes of $\alpha^2 F$.

An informative observation is that, as far as the limiting value goes, neither λ nor ω_2 is separately relevant. Physically, increasing λ decreases ω_2, and there are numerous examples of this. Recognize that performing this limit assumes nothing else happens except that λ increases. This procedure is

nonphysical; making changes that increase λ in turn decrease frequencies due to the increased coupling from electronic states at higher energy. Increasing λ often creates lattice instabilities, so the more strongly coupled material cannot exist. On the positive side, nothing prohibits finding superconductors with increasingly large λ with appropriate frequencies and higher T_c. Further analysis of T_c were given in extended descriptions by Allen (1979, 1980) and Allen and Mitrović (1983).

F. Solidifying the formal theory

1. General remarks

Eliashberg theory providing T_c, the frequency- and temperature-dependent gap $\Delta(\omega, T)$, and more, as previously described and as commonly applied, is based on the common but somewhat *ad hoc* choices of (i) using the DFT mean-field eigenvalues and eigenfunctions as including the essential electronic interaction effects in a static lattice (this choice has no rivals), (ii) from that, the self-consistently determined phonon spectrum including static electronic screening, as obtained from DFT, and (iii) the simple bubble diagrams giving the EP coupling contribution to the electron and phonon self-energies (always consistent with Migdal's theorem). The Hamiltonian then consists of band bare electrons (in the static lattice), bare harmonic phonons oscillating in the frozen electron density (which are nonphysical and ill defined), and (iv) the bare electron—bare phonon coupling due to first-order change in the lattice potential due to atomic motion. This step-by-step ansatz, although seemingly first principles, leaves questions about the full self-consistent treatment of the Coulomb interaction.

A general formulation of the electron-phonon problem based on the full crystal Hamiltonian provided by Allen, Cohen, and Penn (1988) revealed that the combined electron and lattice polarization (and the resulting dynamic dielectric screening function) is the central quantity to be addressed by many-body theory. While treating the polarizations separately has become intuitive and works well for conventional metals, a full treatment might reveal novel processes, and possibly new phases of matter in complex materials.

A rigorous underlying formalism for a complex problem often guides progress even when rigor must be relaxed. DFT provides an excellent example. DFT gives a rigorous foundation for treating the full crystal Hamiltonian in Eq. (2), with a restriction to static nuclei. Beyond the ground state energy and magnetic properties, it is established that the Kohn-Sham band structures are reasonable to good representations of single particle excitations in conventional Fermi liquid metals, as soon as a sufficiently sophisticated exchange-correlation functional is incorporated. This characterization is especially relevant near the Fermi surface of metals, where the necessary corrections can be incorporated when desired.

2. Superconducting density functional theory

Such a formal underpinning for superconductors was devised by Gross and a sequence of collaborators. For this Colloquium we emphasize the density functional theory for superconductors (SCDFT) formulated for material-specific
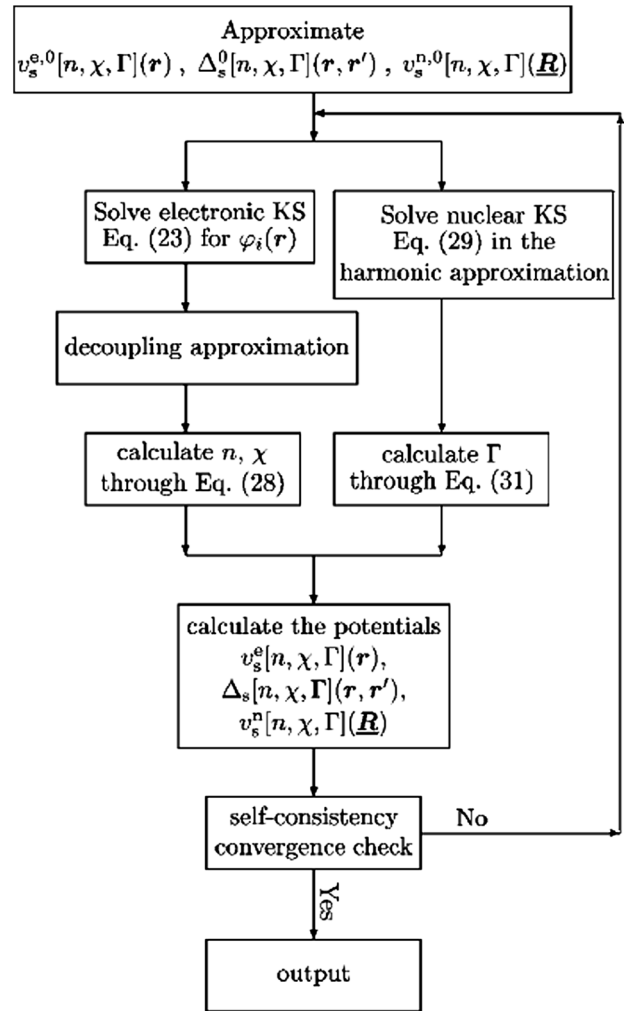
FIG. 6. Flow chart for the *ab initio* (entirely empirical-information-free) calculation for superconducting density functional theory, describing electrons and nuclei in thermal equilibrium in a superconducting state. See the original publication, from which the definitions of various items and the full formalism can be obtained. From Lüders *et al.*, 2005.

studies, which was achieving implementation by 2005 (Marques *et al.*, 2005). The formulation includes a number of innovations, with the basic ones the extension of ground state DFT to thermodynamic DFT, followed by a generalization to a description of quantum nuclear degrees of freedom that then incorporates an allowance for a superconducting order parameter.

Accounting for superconductivity involves a functional $F[n, \chi, \Gamma]$ of the electron density $n(\vec{r})$, the superconducting order parameter $\chi(\vec{r}, \vec{r}')$, and the diagonal of the nuclear density matrix $\Gamma(\{R\})$. The resulting three Euler-Lagrange equations involve one for the nuclear coordinates, of a generalized Born-Oppenheimer type, and two Kohn-Sham Bogoliubov–de Gennes–like equations for the electronic states. Each of the equations involves its own exchange-correlation potential that requires approximation.

In the standard approximation invoking Migdal's theorem, the first equation describes fully dressed harmonic phonons. The formalism is extended to nonzero temperature

thermal equilibrium, finally providing properties of the super-conductor below T_c. Above the calculated T_c, the order parameter and corresponding potential vanish, and the solution reverts to the usual DFT description of the normal state. The schematic flow chart in Fig. 6 provides an outline of the computational program.

Another central feature of SCDFT is that the empirical Coulomb parameter μ^* no longer appears. Instead, the screened Coulomb interaction is calculated from a functional involving the electron dielectric function $\epsilon(\vec{q}, \omega)$ as the central quantity. A few choices for this functional have been tested, analogous to the DFT exchange-correlation functional, which likewise has undergone refinements over several decades.

3. Tests for elemental metals

This formulation with its computational implementation (see the flowchart in Fig. 6) has been shown to be highly accurate for elemental superconductors, especially considering the lack of any empirical input. In the upper panel of Fig. 7 the calculated value of T_c is compared with the experimental value for five elements with significantly different strengths λ and shapes of $\alpha^2 F(\omega)$, all within the 1–10 K range of T_c. For the Thomas-Fermi free electron (or TF-FE) choice of screening functional [see Lüders *et al.* (2005), Marques *et al.* (2005), and Sanna (2017) for details], there is only a negligible error (the maximum is 0.7 K for Ta). This accuracy for low to modest T_c superconductors is impossible when μ^* is uncertain (i.e., is used as an empirical parameter) because the difference $\lambda - \mu^*$ involves both the uncertainty in λ (from approximate functionals and lack of full numerical convergence) and the fundamental uncertainty in μ^*, while the value of T_c is approaching zero because λ is approaching the vicinity of μ^*.

The lower panel in Fig. 7 illustrates a different test of the theory. It displays the calculated $T = 0$ static gap $\Delta(0, 0) \equiv \Delta_0$ compared to the experimental value. The correspondence is somewhat off for the transition metals Ta and Nb, depending on the approximate screening functional that is used, but the theory can be improved with better screening functions, likely at a cost in computational effort. The report (Marques *et al.*, 2005) of these results indicates how the shapes and magnitudes of the electron-phonon spectral function are substantially different for Pb than for Al, Nb, or Ta, yet the theory is highly accurate for all.

4. Application to intermetallic compounds

In the design of and search for new superconductors, improved numerical efficiency is much desired. With such alterations made to the functionals (sometimes with concepts borrowed from models), the procedure was applied by Sanna, Pellegrini, and Gross (2020) to elemental metals, including those mentioned previously, to the transition metal carbide TaC and nitride ZrN, to intercalated graphite CaC_6, to the $A15$ compound V_3Si, to the high T_c boride MgB_2, and to the compressed hydride SH_3. For these compounds the results are much improved, sometimes dramatically (except for ZrN, with T_c predicted to be 3 K too high), compared to the 2005 implementation applied to the same compounds. The variation of T_c in this set of materials ranges from 1 K for Al to 203 K
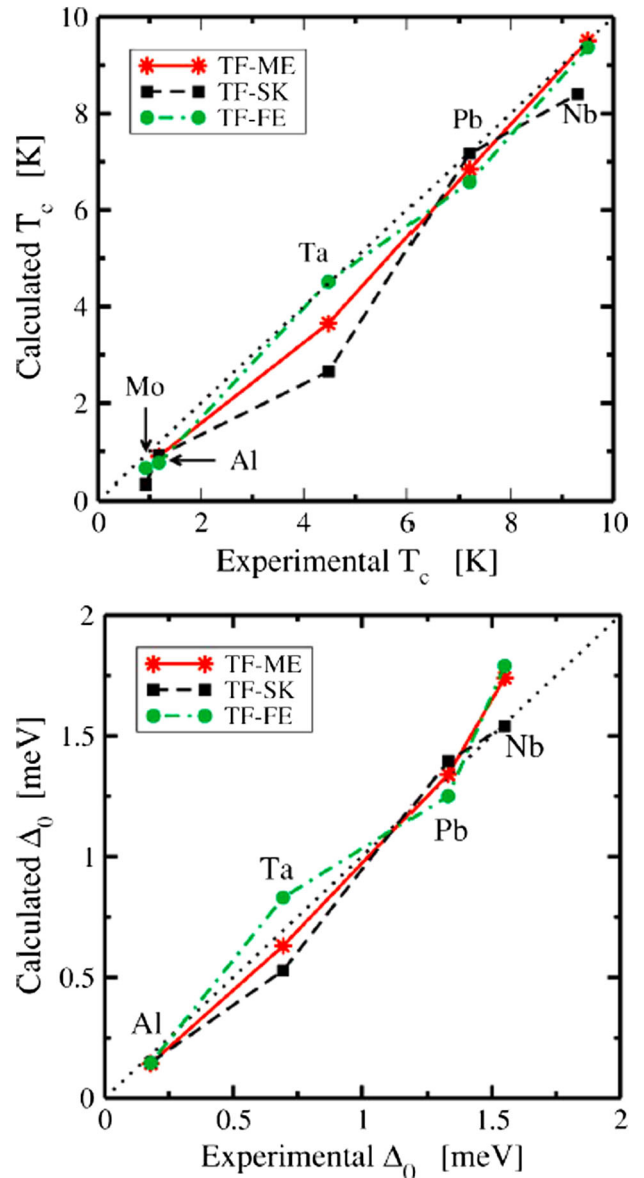
FIG. 7.   Top panel: T_c calculated within SCDFT plotted vs the experimental value. The dotted line along the diagonal indicates perfect agreement. The different piecewise linear lines indicate the use of three different dielectric functions for the Coulomb repulsion. Results for the TF-FE choice are almost indistinguishable from the experimental value. Bottom panel: analogous plot for the zero temperature static energy gap (calculations done at 0.01 K), which can be measured in several experiments. All show extremely encouraging agreement; the Thomas-Fermi–Sham-Kohn (TF-SK) values are somewhat better than the TF-FE values compared to experiment. No information on the Mo superconducting gap (which is small) is available. From Marques *et al.*, 2005.

for SH_3, and the values of calculated λ range from 0.4 to 2.8. A likely area of needed improvement was identified as the functional related to Coulomb repulsion: what one might heuristically associate with μ^*.

Owing to the stated "low computational cost" of the changes allowing substantially improved numerical efficiency, additional capabilities have become available. The full k dependence of the gap over the Fermi surface, a property

of increasing interest especially after the discovery of the strong multigap character of MgB_2, is one such capability.

The point of this section is to emphasize that a fully *ab initio* and unusually accurate calculation of superconducting state properties and T_c has become available for electron-phonon superconductors. The existence proofs of the underlying formalism allow for extended functionals in which the electron-electron interaction plays a more active role in the pairing mechanism.

G. Limitations of SCDFT- or DFT-Eliashberg theory

SCDFT is formally exact for a condensed matter system in thermal equilibrium, in analogy with the formal exactness of diagrammatic perturbation theory. In practice one relies on (1) three functionals: most obviously that of DFT for the static lattice, then those necessary for the superconducting state, and (2) the Migdal theorem, which states that electron and phonon propagators can be treated in the single bubble approximation; vertex corrections (more involved diagrams) are negligible. SCDFT involves approximations of the various functionals that appear when pairing is treated.

1. Anharmonicity, nonlinear EP coupling, and quantum protons

For metallic EP superconductors, the previously outlined theory has reached a level comparable to that for metals in the normal state (though not yet widely applied), whose phenomenology was formalized in Landau-Fermi liquid theory. If the metal is not a Fermi liquid, which can be due to low dimensionality, disorder, or strong electronic interactions, these effects must be built into the functionals. Complications include anharmonicity of the phonons and nonlinear EP coupling, both of which arise diagrammatically as vertex corrections but are not often approached strictly diagrammatically. An example is anharmonicity, which can be folded into a quasiharmonic treatment.

The anharmonicity and its associated nonlinear EP coupling are so pronounced that they can be visualized directly. The Supplemental Material (104) displays the dynamic motion of S and H atoms in a $3 \times 3 \times 3$ supercell of SH_3, obtained from a first principles molecular dynamics simulation of the material at 200 GPa and 200 K, just beyond in pressure where it would have become superconducting. Such simulations are not often studied directly by eyeball (unless with exaggerated displacements), because the motion would hardly be visible, as for S in this simulation. Hydrogen, about 35 times lighter than S, undergoes vibration amplitudes that are large and obvious, even suggesting that melting (at least of the H sublattice) might not be far away in temperature. The large displacement will be accompanied by nonlinear EP coupling effects. Both anharmonicity and nonlinear coupling are being addressed by theory.

Quantum behavior of the nuclei is more prevalent for hydrides due to the light proton mass. Effects on T_c are material dependent. While corrections to T_c from each of these effects are at the $\pm 5\% - 8\%$ level, and further can be either additive or competing, their impact can be more far-reaching in materials with a complex unit cell.

One extreme example of the impact of quantum nature of the proton on structure is provided by LaH_{10} with its clathratelike
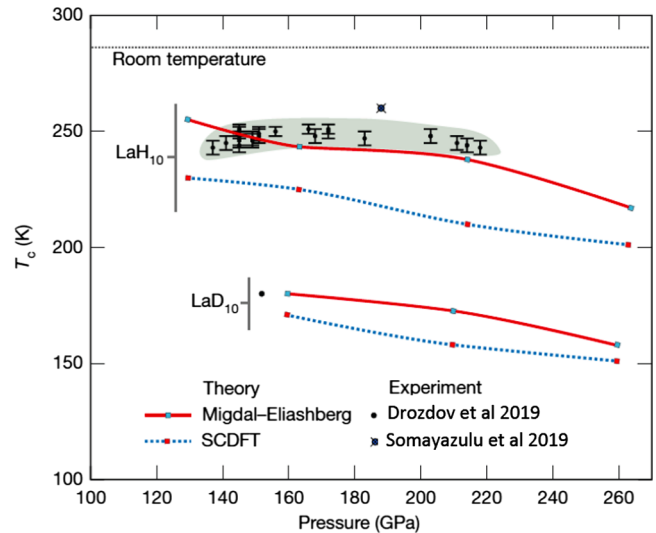

FIG. 8. Calculated vs experimental values of T_c in $Fm\bar{3}m$ LaH_{10} and LaD_{10}. The measured values are shown as dots from Drozdov *et al.* (2019), and as dots with crosses from Somayazulu *et al.* (2019). The solid (red) lines are from an anisotropic Eliashberg calculation, and the dashed blue lines are from SCDFT. Both include anharmonic phonons within a stochastic self-consistent harmonic approximation. Adapted from Errea *et al.*, 2020.

H cages around La. When a classical description of the proton is used, the $Fm\bar{3}m$ structure becomes dynamically unstable below 220 GPa, while it is observed to be a 250–260 K superconductor around 200 GPa and somewhat lower; see Sec. VI for more details and references. Errea *et al.* (2020) found that the enthalpy surface contained several atomic configurations with a lower enthalpy than the $Fm\bar{3}m$ structure, which is inconsistent with the observed structural data. Including the zero-point energy of quantum fluctuations of the proton along with anharmonic corrections, the enthalpy surface reverted to a single minimum at the $Fm\bar{3}m$ structure down to 130 GPa, thus restoring agreement with experiment.

The fully corrected SCDFT results are shown in Fig. 8, along with those from more conventional Eliashberg theory but with the quantum proton and anharmonic corrections included such that LaH_{10} remains stable down to 130 GPa, as found experimentally. The two theoretical curves differ by about 10% for the hydride and 5% for the deuteride, where anharmonic and quantum fluctuation effects would be smaller for the deuteride. For this case, it seems that current SCDFT is not as accurate in reproducing the experimental results (Drozdov *et al.*, 2019; Somayazulu *et al.*, 2019), which might indicate needed improvement in the SCDFT functionals, or might even be accidental given the possible complexities of sample preparation. The comparison in Fig. 8 is with experimental results from two groups (Drozdov *et al.*, 2019; Somayazulu *et al.*, 2019).

2. Eliashberg theory at strong coupling

Over many years there have been studies following the expectation that strong EP coupling alone will provide a breakdown of Eliashberg theory for the normal state.

The question needs to be specified more specifically since the DFT-based Eliashberg theory is a given formalism. In the absence of divergences, it makes specific predictions for the system, and these are what current and past solutions describe.

The implicit question is more likely this: at strong coupling, does Migdal-Eliashberg theory give correct results for known or realistically predicted materials? Conclusions [see Bauer, Han, and Gunnarsson (2011), Chubukov *et al.* (2020), and Schrodi, Oppeneer, and Aperis (2020) for treatments and references] have often been based on the Holstein model, originally put forward as a minimal model treatment of EP coupling, applicable to low density carrier systems, i.e., semimetals and doped semiconductors.

In the Holstein model, the EP interaction is entirely on site: electron charge on a site is coupled to a nonspecific scalar displacement on that site. Intersite coupling is due only to indirect coupling through the conserved charge density; there is no modulation of an intersite hopping parameter. As mentioned in Sec. II.E.3, Allen and Dynes studied T_c in Eliashberg theory to large values of coupling, finding a smooth $T_c(\lambda)$ relation with no evidence of a phase transition, or even a crossover. The question is: At large coupling, does Migdal-based Eliashberg theory cease to provide the behavior of real systems and, if so, how does this happen?

DFT-based Eliashberg theory treats the force on an atom due to its displacement as a collective effect, involving changes in potential that induce forces from neighboring shells that impact, sometimes strongly, dispersion of the renormalized (physical) phonons. An electron mass enhancement fixed to the Fermi energy results in an enhancement of the fermion excitation density of states by a factor $1 + \lambda$. The resulting phonon dispersion determines the possible instabilities of the lattice. Numerically exact (Monte Carlo) and other nonperturbative techniques cannot handle the resulting complications of real materials in currently available computational time. In other words, the strong EP coupling limit based on the full crystal Hamiltonian of Eq. (2) has yet to be attempted.

Experience to date, both experimental and computational, indicates that the primary limitation of DFT-Eliashberg theory derives not from strong coupling *per se*, i.e., electron mass enhancement, but rather from lattice instability that is sometimes already occurring at moderate coupling. There are numerous examples indicating that strong-coupling-related lattice instability, which is strongly material dependent and often Fermi surface related, can already occur at moderate coupling. Phonon branches are renormalized to lower energies in a momentum- and branch-dependent fashion, followed by zero and calculated imaginary frequencies as the coupling strength increases. Calculations up to $\lambda = 4$ (see Secs. II.G.3–II.G.5) indicate that it is possible to have standard EP-coupled systems at that coupling strength (although lattice instability is imminent).

3. Inapplicability of Migdal's theorem

We now return to the more formal limitations of Migdal-based Eliashberg theory. At the most basic level, the regular decrease in importance of successive terms in the perturbation expansion relies (in a self-consistent treatment at a chosen number of terms) on the smallness of the ratio of phonon velocity to Fermi velocity,

$$\frac{\omega_q/q}{v_k^*} = \frac{\omega_q/q}{v_k/(1 + \lambda_k)} \ll 1, \qquad (14)$$

often stated heuristically in terms of the electron-to-ion mass ratio $\sqrt{m/M}$, around $1/300$ for medium mass ions. The ratio of phonon phase or group velocity to Fermi velocity is typically 10^{-2} or smaller in Fermi liquid metals, providing a good expansion parameter. The renormalized (downward, by the EP mass enhancement $1 + \lambda_k$) Fermi surface velocity v_k^* allows for a self-consistent treatment at second-order perturbation theory.

In a given band this velocity might approach zero near E_F due to a van Hove singularity, but typically in a small region of the zone and for a single band out of several, perhaps giving rise to unusual effects but not an invalidation of the theory. The platform of flatband materials provides possible realizations for violations of this condition, but the small phase space in a conventional metal, viz., a wideband compressed hydride (compressed hydrides have occupied conduction bandwidths or 25 eV or more), argues that such occurrences will be rare and, in a many-band background, of minor impact.

Fermi surface nesting, which has an extensive literature, can exaggerate a related condition of this sort, providing a larger phase space in which inter-Fermi-surface scattering acquires a significant phase space. This possibility is real and the resulting behavior of the system (several possible instabilities involving broken symmetries) is material (and model) dependent.

4. Thermal fluctuations at high T_c

Superconductivity theory, especially in the strong-coupling regime, posits a complex-valued order parameter (related to the energy gap function). In bulk EP superconductors fluctuation of the magnitude of the gap is rarely regarded as a limiting factor for high T_c. In quasi-2D high T_c cuprates, fluctuations of the phase of the order parameter have received a great deal of attention, with one viewpoint being that fluctuations are especially large, and possibly limiting, in the pseudogap region of the doping-temperature phase diagram. While fluctuations are much less of a factor in three dimensions than in two, the elevated values of T_c in compressed hydrides invites consideration of the question.

An energy scale for the phase stiffness was given by Emery and Kivelson (1995) as

$$V_o = \frac{(\hbar c)^2 a}{16 \pi e^2 \Lambda_L^2(0)} \qquad (15)$$

in terms of the London penetration depth $\Lambda_L(T)$ at zero temperature and with a characteristic length scale a that would be comparable to the superconducting coherence length. If V_o (in temperature units) begins to approach T_c, fluctuations would begin to arise, requiring a generalization of Eliashberg theory where no fluctuations appear (it is a mean-field theory in this respect).

Eremets *et al.* (2022), Minkov, Bud'ko *et al.* (2022), and Minkov, Ksenofontov *et al.* (2022) provided, from upper and lower critical field measurements, the necessary data for SH_3 and LaH_{10}, with T_c around 200 and 260 K, respectively. The values are, respectively, $a \approx \xi = 1.84 \,(1.51)$ nm and $\Lambda_L(0) = 18.2 \,(14.4)$ nm. A more recent design for

measurement of flux pinning, for different samples of SH_3, gave $\Lambda_L(0) = 27$ nm. In each compound the ratio V_o/T_c is on the order of 10^3–10^4, so order parameter phase fluctuations are negligible in compressed hydride superconductors.

5. Broader comments

The conclusion based on the full DFT-Eliashberg theory and behavior of real materials is that there is currently no established limit on EP-mediated superconducting T_c if the aforementioned vertex corrections are taken into account. A few calculations are predicting above room temperature superconductivity in certain compressed hydrides where the strongly coupled phonons have high frequency and λ exceeds 4. While there is no known fundamental limit, it does not follow that prospects are promising. However, the high T_c regime (versus the more specific but elusive large λ regime) remains open to new discoveries.

The challenge is (i) to retain lattice stability and (ii) to achieve strong coupling to high frequency phonons: both high Ω (an appropriate phonon frequency scale) and large λ. High T_c seems to require a T_c expression that is increasing in both Ω and λ. The theory gives the Allen-Dynes conclusion: the regime of high λ is

$$T_c \propto \sqrt{\lambda \omega_2^2} = \sqrt{\eta/M}. \qquad (16)$$

Somewhat peculiarly, $\eta = N(0)\mathcal{I}^2$ is the purely electronic quantity shown by McMillan to be the vibration-frequency-independent moment of $\alpha^2 F$. This result is subject to vibrational behavior by requiring no unstable modes, but instead an otherwise arbitrary vibrational spectrum. The inverse square root of mass factor is in line with Ashcroft's original proposition (Ashcroft, 1968); hydrogen systems might have an order of magnitude times larger limit than Nb compounds (with other differences depending on η). Recall that the regime of high T_c may not be the same as that of large λ. Hydrides suggest that high T_c is the regime of high frequencies. It is difficult to imagine higher frequencies, except at even higher pressures.

III. APPLYING THE THEORY

With DFT-Eliashberg theory in hand, the periodic table and compilations of known superconductors provide an imposing number of possible applications posing the following question: Which materials systems are the most rewarding for study? This question is discussed in this section, with the question of how to sample the many possibilities given some discussion in Sec. IV.

A. Choice of favorable materials platforms

Regarding ever higher T_c, transition-metal-based materials had been sampled and studied, experimentally and theoretically, by 2010. Promising directions were few, but included organic superconductors and interfacial (excitonic) superconductivity. Considering possibilities more generally, the favored palette of atomic constituents for higher, possibly room temperature, superconductors had already been presented by Ashcroft. In 1968, while research focused on transition metal compounds, he proposed elemental metallic hydrogen as a high T_c material

(Ashcroft, 1968) based on (1) its small mass favoring high frequencies and (2) the vibrating proton without core electrons, which if not too strongly screened should provide the strong scattering that would be required for pairing at high frequencies.

These properties were supported by the BCS equation (1), although little of a material-specific nature was understood relating to higher T_c. Ashcroft understood that it would require high pressure to metalize hydrogen, specifically to break the H_2 molecular bond to create an "atomic hydrogen metal" and bring strong scattering processes to the Fermi energy. That it would require on the order of 1 TPa (10 Mbar) or more (McMahon and Ceperley, 2011) to break the H_2 bond may not have been anticipated.

The theoretical and computational capabilities to address this question would not be available until the next century. In 2004 Ashcroft (2004) refocused his concept, arguing that hydrogen-rich molecules, viz., H_2, CH_4, NH_3, etc., could circumvent the challenge of breaking the strong H_2 bond by replacing it with a weaker bond and also provide "precompression" (higher H density) in the experiment, thereby lowering the required pressure to produce what would essentially be metallic hydrogen. Section V reveals how highly successful this path has been.

B. Computational implementation

The formalism and some important analysis was complete by the mid-1980s, where self-consistent DFT calculations could provide the electron wave functions and band structures giving Fermi surfaces in good agreement with experiment, and phonons were becoming available but were still challenging computationally. The expression for the Eliashberg function, reexpressed from Eq. (3), illustrates one of the computational bottlenecks,

$$\alpha^2 F(\omega) = N_\uparrow(0) \frac{\sum_{k,Q} |M_{kk'}|^2 \delta(\omega - \omega_Q) \delta(\varepsilon_k) \delta(\varepsilon_{k+Q})}{\sum_{k,Q} \delta(\varepsilon_k) \delta(\varepsilon_{k+Q})},$$

where the Fermi energy $\varepsilon_F = 0$ and $Q = k' - k$ is the wave vector of the phonon scattering an electron from state k to $k + Q$, both on the Fermi surface. Necessary sums over bands and phonon branches are implicit.

The sums that are shown are each over the three-dimensional Brillouin zone, confined by the pair of δ functions to lines of intersection of Fermi surfaces, one displaced by Q from the other and requiring fine meshes for convergence. As before, the density of states factor is for a single spin, designated by the arrow on $N_\uparrow(0)$. This expression makes the geometrical interpretation of a double average of $|M^2|$ evident over the line of intersection of two Fermi surfaces with relative displacement $Q = k' - k$, all done in a frequency ω-resolved fashion.

To emphasize the numerical challenge, we note that the EP matrix element $M_{k,k'}$ of Eq. (8) requires the computation of the self-consistently screened potential due to each phonon displacement, then requiring identification and evaluation of the matrix element between electron states k and $k + Q$ on the Fermi surface, with necessary band and phonon branch indices. These are included within the six-dimensional integral. This extensive computation has, through innovative algorithms,

been brought to a viable though still time-consuming level. The electron states are expressed in terms of localized Wannier functions (Mostofia *et al.*, 2008), and the phonons are expressed in terms of localized lattice Wannier functions (Rabe and Wagmare, 1995; Cockayne, 2005). This combination considerably speeds up the various required zone samplings.

Linear response algorithms have been implemented to enable the phonon-induced change in the screened potential to be calculated from the formal infinitesimal-displacement limit. Beyond the basic DFT formalism and codes, evaluating $\alpha^2 F$ to convergence required a sequence of advancements of formalism and a construction of codes, many of which were adapted to parallel computation. In lieu of attempting to describe them, we refer the interested reader to a modern treatment of anisotropy by Margine and Giustino (2013), an extensive review article on the EP formalism with several of the algorithms and references (Giustino, 2017), and a monograph on materials modeling (Giustino, 2014).

IV. CRYSTAL STRUCTURE PREDICTION

A. General recent activities

Section III described the developments that have led to the current capability: given a dynamically stable specific compound, the EP coupling strength λ, superconducting T_c, and several properties of the superconducting state can be reliably calculated. The design of new superconductors requires a separate capability: the prediction of new stable crystalline materials. The design and discovery of new materials were occasional occurrences until the several-agency-wide U.S. program Designing Materials to Revolutionize and Engineer our Future, which was initiated in 2011. Related programs have emerged in other countries.

The idea was to push the ever-expanding computational power, and theoretical and algorithmic development, to design new materials and properties in many classes, to accelerate experimental discovery, and then to speed up the time to market for new products. Many new programs have supported this initiative, which emphasized computational theory-experiment partnership and research, development, and industry synergy.

Materials design, even restricting oneself to crystalline materials with modest sized unit cells, is a challenging process. We begin with the choice of the number of elements (we discuss binaries; ternaries and beyond require thoughtful choices) and their stoichiometry, with some chosen property in mind but initially in the background. A great deal is known about structural phases of elemental materials and the concentration-temperature phase diagrams of several binary compounds, and certain ternary classes at ambient pressure. Given the periodic table of 100 elements (X, Z), there are ~5000 X-Z pairs, dozens of stoichiometries, and, for each, as many as dozens of reasonable structures. For a brute force search, a DFT relaxation would require perhaps 2.5×10^5 compounds, certainly a daunting task. Classification into the 230 space groups can help to organize the exploration, but samples with first-order transformations readily skip over space group symmetries.

The focus in the following is on Ashcroft's suggestion of H-rich materials, which for binaries reduces the search drastically to $\mathcal{M}H_n$ compounds but leaves a still challenging task (here the formula is normalized to one $\mathcal{M}$ atom). Here we start with compressed hydrides, adding the essential pressure variable to the space to be explored. The challenge is to identify candidates that are metallic and thermodynamically stable (metastable phases that are not far from stability may be of interest), then check to determine whether they are dynamically stable. Finally, calculations of electron bands and wave functions and the phonon spectrum, followed by $\alpha^2 F$, are done. Calculations of T_c and $\Delta(\omega, T)$ are then made, and a few other properties of the superconducting state can be carried out using the previously mentioned algorithms and codes.

1. Free energy functional

To identify thermodynamic stability (compounds that will not decompose into two or more phases with lower energy) for any chosen pressure P and temperature T, an efficient numerical scheme is required due to the computational complexity of the exercise. Fundamentally, the goal is to identify, for a given stoichiometry $\mathcal{M}H_n$, the minimum enthalpy $H(P, T)$ over the possible crystal structures. Somewhat more precisely, one really needs for the most precise prediction the minimum of the Gibbs free energy,

$$\mathcal{F}(P,T) = [E(P,T) + PV(P,T)] - TS(P,T)$$
$$\equiv H(P,T) - TS(P,T), \qquad (17)$$

in terms of the internal energy E, enthalpy H, volume V, and entropy S (mostly lattice vibrational at the temperatures of interest).

It is found that the lattice zero-point energy in $E(0,0)$ is more important for hydrogen than for heavier atoms, and the entropy term can shift phase boundaries. The zero-point energy and entropy requires calculation of the phonon spectrum, but much screening of candidates can be done without this step. The volume V and internal structural parameters are relaxed (at $T = 0$) to get the enthalpy $H(P, 0)$, and the vibrational entropy is calculated when that level of precision is desired. When $H(P, 0)$ is plotted versus the concentration of H, the resulting envelope is called the convex hull. The minimum gives the predicted most stable stoichiometry, which is calculated for each pressure of interest.

In the area of compressed hydrides, it has become fairly standard to calculate the complex hull for each pressure of interest, and often to check the most favorable case(s) for dynamic stability. That information makes it worthwhile for the experimenter to attempt synthesis and characterization, and this symbiosis has been evident in several productive collaborations.

B. Evolutionary prediction

An enabling capability in the structural search has been the development in this century of evolutionary crystal structure predictions. There are a few methods in use, but the concept is

to choose a few (or many) candidate structures, relax them, and compare properties, especially the total energy or, under pressure, the formation enthalpy. The most favorable candidates are chosen to guide the construction of new candidates (typically derived "evolutionarily" by some algorithm) until the most favorable candidate is obtained (for a given pair and a given cell or supercell size as a practical limitation).

Crystal structure predictions progressed from early random sampling, basin hopping, and force-field molecular dynamics to first principles DFT-based enthalpy comparisons, often outlining the convex hull of thermodynamic crystal stability. Some prominent modern methods (with clues to the methods contained in their acronyms) include Crystal Structure Analysis by Particle Swarm Optimization (CALYPSO) (Yang *et al.*, 2012)), Universal Structure Predictor: Evolutionary Xtallography (USPEX) (Glass, Oganov, and Hansen, 2006), *Ab Initio* Random Structure Searching (AIRSS) (Pickard and Needs, 2011), and XtalOpt (crystal structure prediction and optimization) (Lonie and Zurek, 2011). These codes incorporate various algorithms from simulated annealing, evolutionary and genetic algorithms, minima or basin hopping, particle swarm optimization, metadynamics, and (quasi)random searches (Hilleke and Zurek, 2022) to search the necessarily broad configuration space. Further information was given by Oganov (2010).

Actual procedures differ, and the likelihood of finding the true stable formation enthalpy minima is constrained by a few factors, such as unit cell size (faced by all methods) and the effort spent to sample the full phase space, which as mentioned is a daunting task. A typical procedure might proceed as follows. After choices of metal atom, H concentration n, and some candidate structures (or space groups), the volume and atomic positions are relaxed subject to the chosen pressure. In early steps faster methods with somewhat lower precision can be used. Evolutionary steps based on the most favorable candidates produce new candidate structures. The candidate structures are combined, using various algorithms, to produce the next level candidates.

The process is continued (a computationally taxing procedure) until negligible improvement is occurring, signaling convergence. The H concentration n is changed and the process repeated; sometimes this is automated. Varying n, which for a given system can involve hundreds of thousands of structures (Hilleke and Zurek, 2022), the "convex hull" delineating the stable compounds in this binary system can be plotted. Examples of the convex hull of LaH_{10} at three pressures are shown in Fig. 9(a). This method, involving enthalpy calculated from DFT, has proven to be successful in predicting stable candidates. Various chosen pressures must be computed independently.

Thermodynamically stable candidate structures then must be checked for dynamic stability (the absence of imaginary frequencies) to be valid predictions. Stability can be determined either by phonon spectrum calculations or by *ab initio* molecular dynamics. Only then can DFT-Eliashberg theory be applied to obtain T_c and a selection of other desired properties obtained from the gap equation. The procedure for a full search for high T_c is outlined in schematic form in Fig. 9(b).

C. Machine learning and data mining

As in many of the sciences and elsewhere, machine learning techniques are being applied to materials design, but few techniques with applications to compressed hydrides have yet been applied. The basic idea is pattern recognition: provide a large database to give the neural net the opportunity to identify certain characteristics ("training") that are statistically related to given descriptors. An application of the trained apparatus to new possibilities produces likely candidates for the desired characteristics [viz., $T_c(P)$], with rectitude estimated using various statistical measures. While earlier applied to address other materials properties, applications to general superconducting materials have been implemented only more recently. A large database of known superconducting materials exists, consisting of the compound formula, crystal structure, and T_c. However, no experiment-derived database for compressed hydrides exists due to the dearth of hydride examples, so training must be done on computationally predicted cases.

In 2017 an example of machine learning related to superconducting T_c was provided by Stanev *et al.* (2018). They covered a large range of values of T_c and the SuperCon database of more than 12 000 superconductors to provide training.[2] With additional guidance of materials properties from the AFLOW repository (Curtarolo *et al.*, 2012), the procedure was applied to the entire Inorganic Crystal Structure Database (Bergerhoff *et al.*, 1983). More than 30 noncopper and noniron materials, with all being multicomponent oxides, were identified as the most promising candidates.

The machine learning study of hydrides by Hutcheon, Shipley, and Needs (2020) provides a more specific instructive example. For descriptors for candidates MH_n, they chose H content (n), and the metal element (M) size (van der Waals radius), atomic number, mass, and electronic configuration (number of s, p, d, and f electrons). Notice that these descriptors have little direct relation to the quantities that determine λ, phonon frequencies, or interaction strength. Their result identified the first three columns of the periodic table as best candidates for M, a feature also noted in various hydride overviews.

These low electron affinity elements give up much or even all of their valence electrons to the H sublattice. This added charge raises the H $1s$ occupation above the half-filled level, promoting metallicity. In studies of atoms M across the entire periodic table, a few outliers exist: atoms with open d or even f shells. The first discovery SH_3 is a different sort of outlier, with sulfur's open, roughly half-filled p shell. Also unusual for SH_3 is the sharp van Hove singularity at the Fermi level, which could contribute to it being an outlier (Quan, Ghosh, and Pickett, 2019).

---

[2]DICE: a data platform for materials science. National Institute of Materials Science, Materials Information Station, SuperCon: https://dice.nims.go.jp/services/MDR/ (2011).
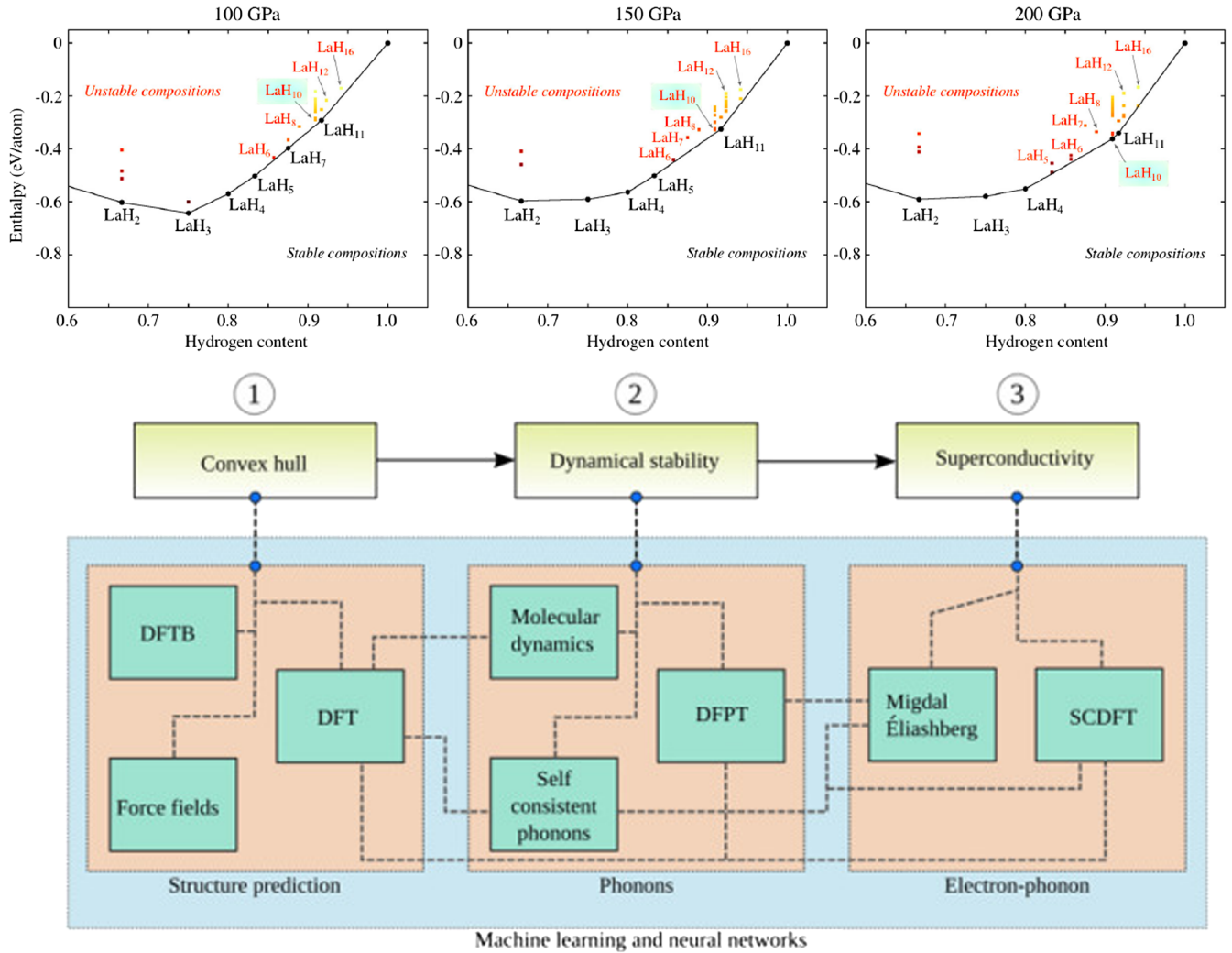
FIG. 9.   Top row: for the LaH$_n$ system, the computed convex hull, with specific calculated formation enthalpies with respect to elemental La and H$_2$. The three top panels display pressures of 100, 150, and 300 GPa for the stoichiometries that were obtained in the search. LaH$_{10}$ is the compound of most interest, marked with a light green (gray) background. Convex hulls often result in several compounds near the convex hull and may be obtained from hundreds or thousands of enthalpy calculations. Adapted from Errea *et al.*, 2020. Bottom row: schematic diagram of the progression of the high T_c search program. First, the thermodynamic stability is obtained from compounds on the convex hull. Second, the dynamic stability is studied and phonon spectra are obtained. Third, the DFT-Eliashberg calculation, EP coupling and the phonon spectrum, is made to obtain $\alpha^2 F(\omega)$, and T_c is obtained from the Eliashberg equation or from one of the fit expressions $T_c(\lambda, \mu^*, \omega_{\log}, \omega_2)$. DFTB, DFPT, and SCDFT indicate separate DFT-based capabilities. Adapted from Flores-Livas *et al.*, 2020.

V. THE BREAKTHROUGH DISCOVERIES: THEORY THEN EXPERIMENT

A. High-pressure experimentation

According to the original concept of Ashcroft (1968), metallic atomic hydrogen should provide the acme of T_c since the atom has the smallest mass, with the highest frequencies if force constants are strong and the potential for strong scattering of electrons by proton displacements that seemed likely to Ashcroft. Calculations sometimes including the quantum nature of the proton have predicted the stable structures versus pressure. The predictions are T_c of 500 K or higher (McMahon and Ceperley, 2011), requiring pressures of 500 GPa or higher. Few attempts have reached a static

pressure this high, so Ashcroft's second suggestion (Ashcroft, 2004) has been the avenue of choice: use H-rich molecules as the ambient pressure sample to avoid strong H$_2$ bonding and antibonding states being pulled away from the Fermi level, and to exploit precompression (higher H concentration and density).

Another point merits mention. Over recent decades there have been reports of signals of possible room temperature superconductivity, usually in resistance or susceptibility measurements, which is the most straightforward evidence of superconductivity. The samples were invariably polycrystalline, multiphase, or disordered to the point of amorphous. Transport and magnetic measurements often show anomalies in such samples. When such signals are not reproducible, they
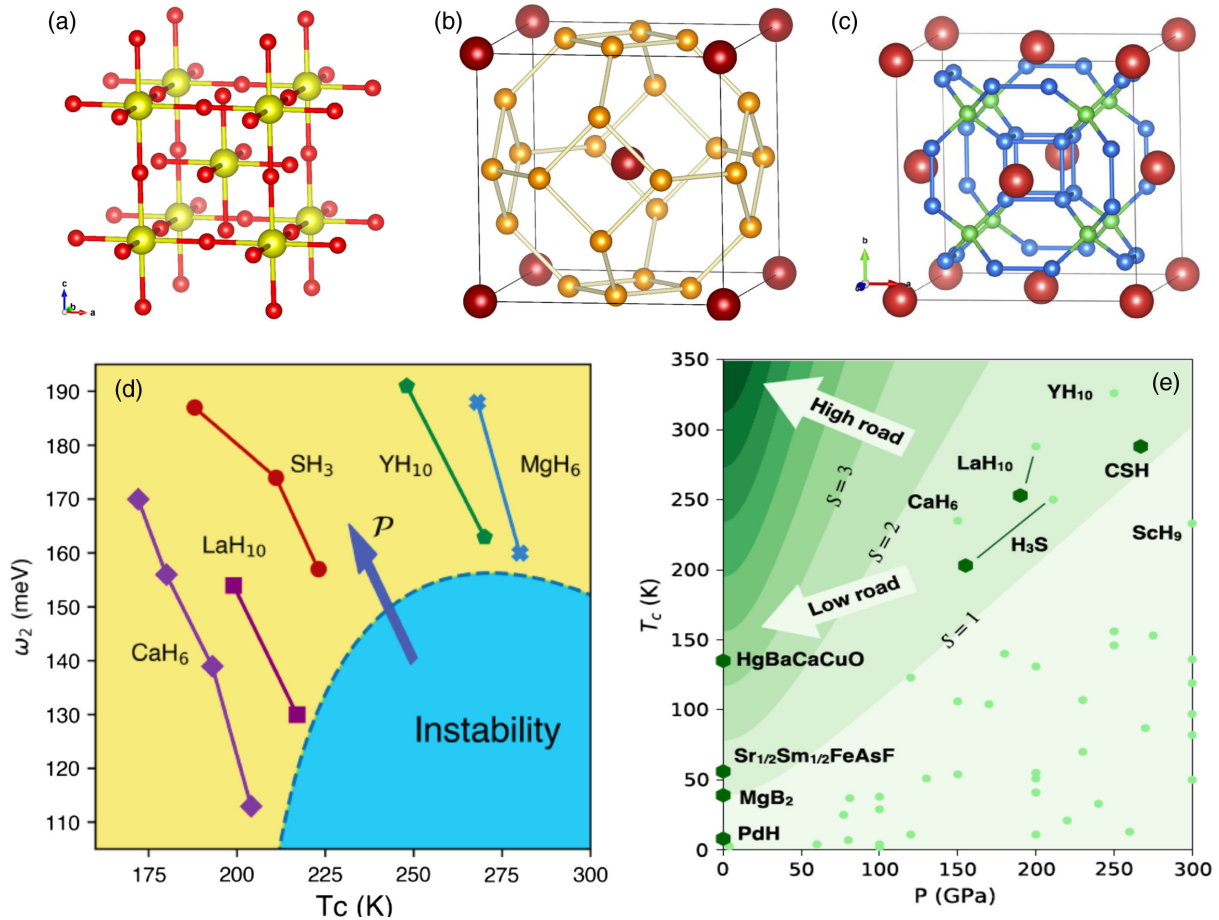
FIG. 10.   Structures of (a) SH_3, (b) YH_6, and (c) LaH_{10} illustrating the high symmetry and the progression toward sodalite- or clathrate-type structures with increased H content. Small circles indicate H atoms, while larger circles denote metal atoms. (d) Schematic ω_2–T_c phase diagram of calculated results for five compressed hydrides in the three crystal structure classes shown in (a)–(c). Note that pressure $\mathcal{P}$ is increasing in the upper left direction, the blue region (lower right region) denotes the low-pressure region of instability of the structures that are considered. Solid lines connect values of a compound changing with pressure. Pressure lowers T_c; as pressure increases, ω_2 increases but λ and T_c decrease. Lowering pressure increases T_c (and λ) but leads to dynamic instability. The trends suggest an "island of instability" (blue region) for compressed hydrides. (e) Pickard's scatterplot in the P-T_c plane of experimental (hexagons) and theoretical (circles) positions for several superconductors. The contours indicate values of the *ad hoc* figure of merit $S = T_c(K)/[T_{c,\mathrm{MgB_2}}(K)^2 + P(\mathrm{GPa})^2]^{1/2}$, which focuses attention on the desirability of low pressure P for higher T_c; see Sec. 12 of Boeri *et al.* (2022).

have made the community skeptical to the point that USO, for unidentified superconducting object, is a recognizable acronym. It is possible that some of them could be evidence of interface superconductivity or some other unusual type, but if not reproducible a report does not receive extensive notice.

For this reason the discoveries that follow focus on reproducible results, noting confirmation. Recognize, however, that the samples in diamond anvil cells are far from the ideal single crystals that are often available at ambient pressure. The compounds are synthesized within the small pressure cell at megabar pressures, as temperatures up to 2000 K are varied. The resulting samples will typically be polycrystalline, strained, and possibly multiphase, and with hard-to-determine stoichiometry. For first-order phase transitions the free energy barriers may be high, making it challenging to reach certain Gibbs free energy minima. For these reasons confirmation of these first three discoveries of approaching or near room temperature superconductivity is

noted. In addition, given the previously mentioned complexities of samples at a given P and T, experimental data will not be uniform across groups, nor even across a given laboratory's runs. Thus, "reproducibility" and comparisons with theoretical predictions should be interpreted accordingly.

B. SH_3: The initial breakthrough

1. Theory

In 2014 Li *et al.* (2014) employed the CALYPSO structure prediction code (Yang *et al.*, 2012) to identify candidate structures with SH_2 stoichiometry at high pressure. Note that this formula is isovalent with H_2O, and the molecules are isostructural. The much more strongly bonded H_2O is known to remain insulating up to the highest static pressure currently available. Their study, finding insulating structures at lower pressures, focused on a transition between two predicted metallic structures in the 130–160 GPa region. The lower

pressure compound has a low symmetry $P\bar{1}$ space group, polymeric structure, with an atomic H *Cmca* phase with a layering of H and S atoms occurring at higher pressure. The calculated T_c was maximal at the transition ($\sim$160 GPa), around 60 K in the $P\bar{1}$ structure and 82 K for *Cmca* and decreased with pressure in the latter phase. The maximum coupling strength, occurring at the structural transition, was $\lambda = 1.25$, with 40% attributed to S modes (which compose 1/3 of the phonon branches).

Appearing immediately thereafter, also in 2014, was a prediction by Duan *et al.* (2014) that for a SH_3 stoichiometry [labeled at the time after the initial constituents as $(H_2S)_2H_2$, and later as H_3S] the high symmetry, atomic H structure pictured in Fig. 10(a) was predicted to be the most stable one in the 150–200 GPa range. The calculated T_c peaked just above 200 K near the lower pressure range in the 160–200 GPa region. A coupling strength $\lambda = 2.2$ was calculated, with 25% arising from the low energy S modes. The cubic structure has one of the highest symmetries possible for this stoichiometry: SH_6 octahedra in a body-centered arrangement are connected on two sublattices by H atoms, which are coordinated only with two S atoms; see Fig. 10(a). Such a remarkably high prediction must have seemed to most to be beyond comprehension, yet it was based on successful structure search algorithms and the established DFT-Eliashberg theory. A theoretical study of sulfur hydrides was confirmed and extended in 2015 by Akashi *et al.* (2015) and Errea *et al.* (2015), who promoted the understanding of the relation of electronic structure and microscopic processes to promote high T_c.

2. Experiment

Independently, experimentalists were working on S-H samples. Even in 2014, Drozdov, Eremets, and Troyan (2014) posted a notice of pressure-induced T_c up to 190 K in sulfur hydride samples, and in 2015 the published announcement (Drozdov *et al.*, 2015) was of T_c as high as 203 K around 160 GPa in the H-S system. The superconductor responded to the magnetic field in the anticipated way, revealing the expected critical field $H_c(T)$ behavior versus temperature.

The sample was later determined by Einaga *et al.* (2016) to have the bcc S sublattice predicted by Duan *et al.* (2014), and it was concluded, based also on computational input and experimental volume, to be bcc SH_3, as shown in Fig. 10(a). The hydrogen → deuterium isotope shift of T_c was large, as theory predicted, and T_c versus pressure was reproduced. This discovery opened the field to the realistic possibility of room temperature superconductivity. High T_c in this *T-P* regime was confirmed by Huang *et al.* (2019), who reported susceptibility measurements T_c as high as 183 K around 150 GPa.

Magnetic measurements by Eremets *et al.* (2022), Minkov, Bud'ko *et al.* (2022), and Minkov, Ksenofontov *et al.* (2022) led to the superconducting materials parameters $\Lambda_L \sim 18$–27 nm and $\xi = 18.4$ Å. The resulting Ginzburg-Landau parameter $\kappa_{GL} = \Lambda_L(0)/\xi(0) = 10$–15 indicates strong type II superconductivity.

There was significant skepticism about SC at 200 K until the following two higher T_c discoveries were made and

reproduced. However, for those who understood the degree and accuracy of the computational theory, the fact that experiment agreed with theory would have been convincing in itself.

C. LaH_{10}: Approaching room temperature

1. Theory

The success of design and discovery for SH_3 emboldened the superconducting materials design community. Binary hydrides $\mathcal{M}H_n$ were the focus. Varying the metal $\mathcal{M}$ atom (valence, size, and chemistry) and moving toward super-hydrides ($n > 6$, say) would seem to approach the optimal combination to move toward the idealistic case of Ashcroft's metallic hydrogen.

In 2017 two theoretical groups, Liu *et al.* (2017, 2018) and Peng *et al.* (2017), nearly simultaneously predicted $\mathcal{M}H_{10}$, with isovalent $\mathcal{M} = $ La and Y, to have high T_c in the 275–325 K range depending on element and pressure (always above 200 GPa). Liu *et al.* calculated $\lambda = 2.2$, with T_c around 265 K. The structure again was the highest symmetry possible for this stoichiometry, cubic with a clathratelike shell of 32 H atoms surrounding the metal atom on its fcc sublattice [pictured in Fig. 10(c)]. Values for λ were in the 2.2–2.6 range, which is similar to SH_3 but also similar to Pb-Bi-Tl alloys from the 1970s with a maximum $T_c = 9$ K that is 35 times lower (Allen and Dynes, 1975). The differences in T_c are due to the high H vibrational frequencies (Ashcroft's primary point) while strong coupling to Fermi surface electrons is retained.

Further studies of this superconductivity were provided by Liu *et al.* (2019) and the quantum (zero-point motion) nature of the structure by Errea *et al.* (2020), as discussed in Sec. II.G.1. Theoretical work by Ge, Zhang, and Hemley (2021) indicated that doping LaH_{10} by B or N on either the La or H site at the few percent level might raise T_c by 30 K, i.e., to $T_c \approx 290$ K, in the 240 GPa regime. This doping also strongly tends to drive the alloys toward lattice instability, a common occurrence when coupling is increased.

2. Experiment

The superconducting materials discovery (experimental) community was also stimulated by the developments on SH_3. Synthesis and evidence of superconductivity in lanthanum superhydride around 260 K was announced in two publications (Geballe *et al.*, 2018; Somayazulu *et al.*, 2019) in 2018 and 2019. Resistivity drops occurred in the 180–200 GPa range for various runs upon cooling and heating, and x-ray diffraction established the fcc sublattice of La, as in the LaH_{10} structural prediction. Superconductivity was confirmed by Drozdov *et al.* (2018), initially at 215 K but soon thereafter up to 250 K (Drozdov *et al.*, 2019). The latter paper reported vanishing resistivity around 170 GPa, a H isotope effect, T_c decreasing with applied magnetic field, and evidence of the predicted crystal structure.

Magnetic measurements by Eremets *et al.* (2022), Minkov, Bud'ko *et al.* (2022), and Minkov, Ksenofontov *et al.* (2022) were noted in Sec. V.C.2. Drozdov *et al.* (2018) introduced a new measurement technique probing flux pinning in small

samples. For LaH$_{10}$, the behavior was characteristic of conventional type II behavior, with the derived values of $\Lambda(0)_L = 14.4$ nm, $\xi = 1.5 - 1.8$ nm, and a Ginzburg-Landau parameter $\kappa_{\mathrm{GL}} \approx 9$.

D. Yttrium superhydrides: The third discovery

1. Theory

The Y-H system has a more extensive history than S-H or La-H systems, partly because some of the design of La-H materials included the isovalent Y-H system. Li *et al.* (2015) reported materials design for this system soon after their 2014 work on SH$_2$ discussed in Sec. V.B. Their 2015 structure search at high pressure identified YH$_3$, a body-centered tetragonal YH$_4$ lattice with both atomic H sites and H$_2$ units, and bcc YH$_6$ with a sodalite structure [Fig. 10(b); Y surrounded by 24 H atoms] as promising candidates. The last two had predicted T_c around 90 and 260 K, respectively, in the low 120 GPa pressure range.

The YH$_6$ prediction was startling on two counts: the predicted T_c was 30% above the already noteworthy SH$_3$ value of the previous year, and the required pressure was somewhat lower. YH$_6$ contains some strongly coupled H modes at comparatively low frequency (not far from instability), accounting for $\lambda \approx 3$ and high T_c in spite of the significantly lowered phonon energy scale $\omega_{\log}$ [the logarithmic frequency moment (Allen and Dynes, 1975)]. However, anharmonicity and nonlinear EP coupling can change predictions, especially when there are nearly unstable modes. These stoichiometries have not been reported in experimental studies to date.

Peng *et al.* (2017) proposed a focus on hydrogen clathrate structures as a route to RTS. Results were presented for $\mathcal{M}\mathrm{H}_n$ structures with $\mathcal{M} = \mathrm{Y}$ and La for $n = 6$, 9, and 10, and $\mathcal{M} = \mathrm{Sc}$ for $n = 6$ and 9. The results pertinent to this discussion are for two yttrium hydrides. YH$_9$ at 150 GPa has the largest calculated coupling: $\lambda \approx 4$ and $T_c \approx 250$ K. However, YH$_9$ at 400 GPa has an even larger predicted T_c: $T_c \approx 290$–300 K with a smaller $\lambda \approx 2.3$. Considering the differences in structures and in optimum pressures, even their substantial amount of data only begins to provide guidelines for just what factors are most important in promoting RTS.

In 2019 Heil *et al.* (2019) predicted clathratelike structures from their structural search, focusing on YH$_6$ and YH$_{10}$. The results for YH$_6$ were similar to those of Li *et al.* (2015), with calculated anharmonic effects accounting for some of the differences. T_c was predicted to be similar (275 K) for YH$_6$ at 100 GPa, an encouraging result for the efforts to produce and retain high T_c hydrides at more accessible pressures. For YH$_{10}$ a predicted $T_c = 300$ K around 300 GPa was obtained, which is similar to the results of Peng *et al.* (2017).

For this compound a large coupling $\lambda \approx 4.5$ was reported, reproducing reasonably well the results of Peng *et al.* (2017). This value is among the largest values from DFT-Eliashberg theory for a real (if still only predicted) compound. This large value of λ benefits from soft phonons, that is, being close to a dynamical instability, which is a typical occurrence in several crystal classes (Quan, Ghosh, and Pickett, 2019). When this occurs, corrections for anharmonicity, quantum fluctuations of H, and nonlinear EP coupling become necessary to pin down the critical pressure for instability as well as for the most complete prediction of T_c. Generally, but especially in hydrides, low frequency modes do not promote T_c as much as their contribution to λ would suggest (Quan, Ghosh, and Pickett, 2019; Boeri *et al.*, 2022); see Sec. VI.B.

2. Experiment

Experimental verification of the prediction of high T_c in the yttrium hydride YH$_9$ was announced in 2019 (Kong *et al.*, 2019) and published in 2021 (Kong *et al.*, 2021) as $T_c = 243$ K at 200 GPa in space group $P6_3/mmc$, with the expected structure being clathratelike. The compound YH$_{10}$ predicted to have higher T_c was not observed in their experiments, which covered certain regions of phase space up to 410 GPa and 2250 K. Snider *et al.* in 2021 provided data (Snider *et al.*, 2021) indicating T_c up to 262 K for a sample with a superconducting phase of stoichiometry likely close to YH$_9$ based on Raman data. This maximum T_c occurred around 180 GPa. Extension and some degree of confirmation was provided when $T_c = 253$ K was obtained in $(\mathrm{La}, \mathrm{Y})\mathrm{H}_n$ mixtures by Semenok *et al.* (2021).

As mentioned, other regions of the Y-H phase diagram have been predicted to display high temperature superconductivity. In 2021 Troyan *et al.* reported (Troyan *et al.*, 2021) T_c up to 224 K at 166 GPa in cubic $Im\bar{3}m$ YH$_6$. This compound is an example of strong effects of anharmonicity due to the structure and the small proton mass. The calculated values are $\lambda = 2.4$ using harmonic quantities, reduced to $\lambda = 1.7$ with anharmonic corrections. Anharmonicity considerably hardens the lower frequency H phonons, giving a calculated value of $\omega_{\log} = 115$ meV and T_c in a range of 180–230 K that depends on some choices. Nonlinear coupling corrections may be important to obtain the best predictions. Items to be aware of when comparing predictions with data are noted in Sec. V.A.

VI. CURRENT CHALLENGES

A. Further theoretical guidance

The progress in raising T_c over 11 decades is illustrated in Fig. 1. The lesson of the past was that increases in T_c cannot be foretold. On the other hand, the discovery of new superconductors with T_c approaching room temperature in compressed hydrides has been enabled by material-specific theory and computational materials design, after which near room temperature superconductivity was predicted, then verified by experiment. Intense effort continues toward discovering higher temperature or more accessible superconductors. Given the rapid progress, the way forward suggests optimism, with some understanding of the microscopic processes being partnered by computational power in the search. Considering that the full DFT-Eliashberg results can be dug into at any level of detail that one desires, one can expect helpful understanding to soon begin to emerge. Section VI.B indicates the current level of understanding and identifies the direction needed for further analysis.

In Secs. V.B–V.D, some of the calculated values of EP coupling strength λ for the verified hydrides (and some others)

were mentioned. The superconducting hydride sample is small, but it has already been clear that λ in itself is an unreliable indicator of T_c; increasing λ should not be the primary goal. Past examples show that, within a given structure, λ is increased by lowering frequencies, which leads (often quickly) to lattice instability. Indications from Allen-Dynes analysis (Allen and Dynes, 1975) through more recent studies (Quan, Ghosh, and Pickett, 2019) indicate that increasing the electron-proton scattering matrix element $\mathcal{I}_H$ should become the focus of attention, always assisted by large $N(0)$.

Practically nothing is understood at present about what keeps $\mathcal{I}^2$ large in the RTS materials when the electron gas is being compressed to higher density, and in the simplest picture should be screening more strongly, thereby reducing $\mathcal{I}^2$. $N(0)$ itself is usually normal in size, which may help to promote stability. Several groups have noted that the H-atom DOS $N_H(0)$ per unit volume is likely to be the relevant quantity, but it does not seem to correlate strongly with T_c.

With leadership in materials design by the theoretical and computational modeling communities, and materials discovery by high-pressure experimenters with increasingly advanced techniques, the six-decade-old hope for room temperature has essentially been achieved: T_c up to the 250–260 K range was reproduced and accepted by 2020, in substantial measure due to agreement with prediction. The hurdle for closer study and application is that 150–250 GPa pressure is required. This observation directly suggests two future primary goals: (1) yet higher T_c at high pressure, and ultimately superconducting atomic hydrogen, for the advancement of scientific achievement and the knowledge base and (2) producing or retaining high temperature superconductivity (HTS) to much lower, or preferably even ambient, pressure for applications. The following comments provide items that could lead to advancement toward these goals. Some progress in these areas is noted in Secs. VI.B–VI.D.

B. Analysis of H coupling

Analysis of strong EP coupling strength, especially at high frequency, is crucial in understanding how to increase T_c, as long as it contributes both to the frequency scale and to λ, and also helps to avoid structural instability. However, accomplishing this in compounds is more involved and less transparent than in elements because the relevant quantities [$N(0)$, matrix elements, masses, and phonon frequencies] are mixtures of the constituent atoms and their interplay.

Hydrides are special, besides their high T_c, because the large difference in the metal mass and the proton mass separates the phonon spectrum $F(\omega)$, and hence the Eliashberg spectral function $\alpha^2 F(\omega)$ into separate frequency ranges: low frequency metal acoustic modes separated by a gap from high frequency H optic modes (Quan, Ghosh, and Pickett, 2019). This separation of frequency regions allows the isolation of contribution from each atom

$$\lambda = \lambda_{\mathcal{M}} + \lambda_H, \quad \lambda_X = \frac{N_H(0)\mathcal{I}_X^2}{M_X \omega_{2,X}^2} \quad (18)$$

for X equal to metal $\mathcal{M}$ or hydrogen H. This procedure extends the productive analysis of elemental superconductors
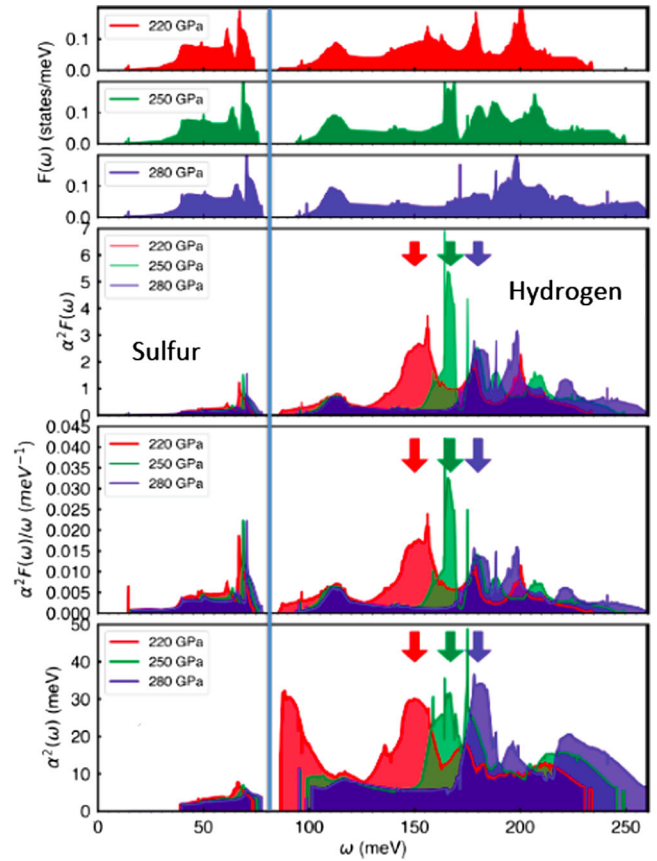

FIG. 11. Color-coded plots of several spectral functions of SH_3 at the three pressures indicated in the top three panels, all above the optimum pressure of 160 K. The main point is to illustrate the separation of S and H modes (the solid vertical line at 80 meV), allowing analysis distinct from their coupling strengths and contribution to T_c. The blue (solid) vertical line marks this separation, lying in the gap around 80 meV between S (left, low frequency) and H (right, high frequency) vibrational modes. Top three panels: phonon density of states $F(\omega)$ for each of the three denoted pressures. The main effect of pressure is to push some H modes to higher frequency. Bottom three panels: $\alpha^2 F(\omega)$, $\alpha^2 F(\omega)/\omega$, and the ratio $\alpha^2(\omega) = \alpha^2 F/F$ that indicates the mean coupling matrix elements' strength at frequency ω, respectively. The arrows indicate peaks of interest. The low frequency region is subject to numerical noise and carries little weight, so it has been cut out. From Quan, Ghosh, and Pickett, 2019.

to allow identification of the individual atomic contributions for compressed metal hydrides. The contribution of the metal atom (discussed later) is enlightening. The comparison of hydrogen contributions and the individual components contributing to λ for the various hydrides becomes possible, with an example given in Fig. 12.

This separation is shown for the spectral function of SH_3 in Fig. 11. The separation of the degree of participation is almost complete. Whereas it has been common to quote the separate metal and H contributions to λ, as previously quoted for a few examples, the capability of separating all of the atomic information is available from $\alpha^2 F$. This deeper analysis is important because λ alone is a poor indicator of T_c. Of prime interest is the contribution to T_c (versus λ, the energy gap, or other properties) from each atom.
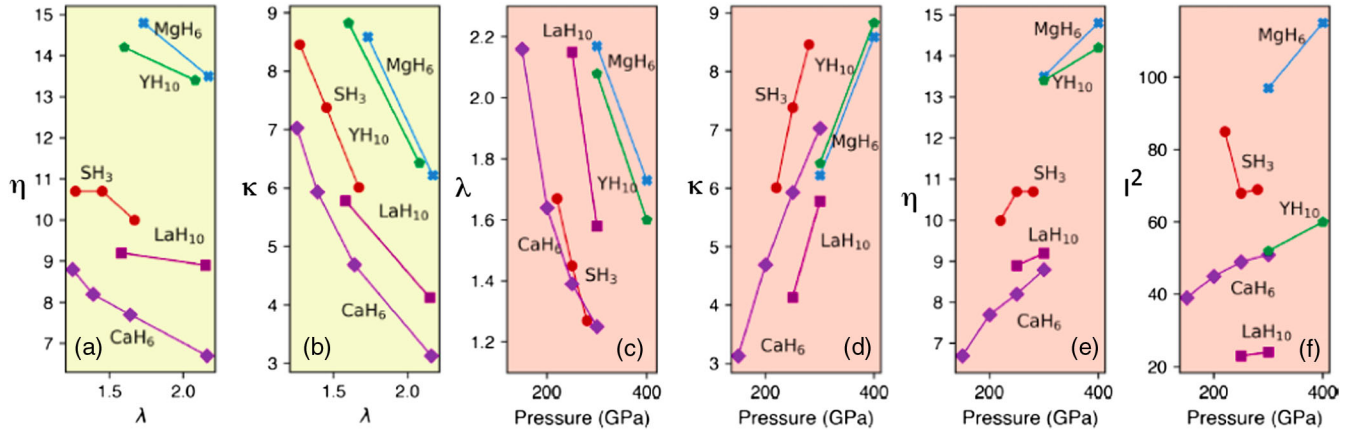
FIG. 12. Atomic H quantities in the indicated superconducting compressed hydrides, obtained by taking advantage of the spectral separation of metal acoustic modes and H optic modes. The corresponding calculated values of T_c are shown in Fig. 10(d). (a) (η, λ) and (b) (κ, λ) phase planes, indicating small and large relative variations. (c)–(f) Pressure variations of the indicated quantities showing the magnitudes and rates of variation with pressure. Units: λ, unitless; $\eta = N(0)\mathcal{I}^2$ and $\kappa = M_H\omega_2^2$, eV/Å^2; $\mathcal{I}^2$, eV^2/Å^2. The background colors (different shadings in gray scale) indicate the different types of plots; see the axis labels. Adapted from Quan, Ghosh, and Pickett, 2019.

An analysis based on the frequency separation of metal and H modes was given by Quan, Ghosh, and Pickett (2019) for five binary hydrides from three crystal structure classes. Figure 10(d) illustrates some aspects of the analysis. A primary indication is of a rough phase boundary identifying an island of instability in the high T_c, but a lower ω_2 regime. Within a high T_c phase, this instability is encountered as pressure is lowered, with λ and T_c increasing until instability is reached. For brevity, only a few other results of this trend study are discussed here.

The first observation in this study is startling. Although it is an appreciable fraction of λ, the metal atom contribution to $\alpha^2 F$ affects T_c only slightly, and sometimes lowers it. This occurs because coupling to low frequency vibrations lowers the phonon frequency scale [the prefactor in T_c in Eqs. (1), (10), and (12)], offsetting the increase in λ. Quan, Ghosh, and Pickett (2019) explained why this does not violate the Bergmann-Rainer "theorem": additional coupling at one frequency affects the phonon spectrum and coupling at other frequencies. This conclusion can be confusing because the metal contribution to λ is evident and often emphasized, while the effect on the frequency scale is never calculated, therefore remaining invisible. This result focuses attention for analyzing and understanding T_c on hydrogen alone (neglect the metal), thereby providing a focus for a more transparent understanding of T_c in terms of hydrogen properties.

The second observation follows from the first: $N_H(0)$ and $\omega_{2,H}^2$ are calculated and the mass M_H is fixed. This makes it possible to extract and analyze the least understood but yet important quantity: the matrix element $\mathcal{I}_H^2$ factor in Eq. (18) for scattering electrons from the moving H atom. Quan, Ghosh, and Pickett (2019) provided a discussion of this and several other aspects of EP coupling in their five chosen compounds, arguing that an understanding of $\mathcal{I}_H^2$ is the main missing link in the understanding of EP coupling in compressed hydrides. A synopsis of some of their analysis

is shown in Fig. 12. In the (η_H, λ_H) phase plane of Fig. 12(a) and the pressure dependencies of η_H and I_H^2 in Figs. 12(e) and 12(f), respectively, the example hydrides seem to self-organize into groups. In the κ_H, λ_H plane and the other two pressure dependencies, the magnitudes and pressure behaviors of the five phases show considerable overlap but clear trends. Note that $\mathcal{I}^2$ tends to increase with pressure, but the magnitudes at 300 GPa differ by a factor of 3.

As mentioned, the strong tendency for $\mathcal{I}^2$ to increase with pressure is counterintuitive since the increased electronic density under volume reduction would seem to provide an increased screening of H motion. This should reduce the $\mathcal{I}_H^2$ factor given in Eq. (8). The change in potential due to H displacement can be evaluated within linear response theory, either from the dielectric constant with all local field terms (highly intensive numerically) or numerically from linear response, which is the method of choice and is still computationally intensive enough to sometimes limit Q phonon point grids.

The pressure increase in $\mathcal{I}_H^2$ indicates that there is more physics to be understood. One can compare this to a simple and efficient approximation from Gaspari-Gyorffy theory (Gaspari and Gyorffy, 1972), which uses a rigid atomic potential displacement model. The result requires negligible computation but involves phase shifts of the potential that provide only a limited physical understanding. The Gaspari-Gyorffy model was applied to SH_3 by Papaconstantopoulos *et al.* (2015), indeed finding that η_H^{GG} also rises steeply and nearly linearly from 18 eV/Å^2 at 200 GPa to 25 eV/Å^2 at 300 GPa. The underlying mechanisms remain unclear. The calculations of Quan, Ghosh, and Pickett (2019) were not extended to higher pressure, so a more complete comparison is not available. Hutcheon, Shipley, and Needs (2020) used Gaspari-Gyorffy theory to give a quick estimate of η in their machine learning study.

C. How to produce strong H coupling

1. The metal-induced atomic hydrogen paradigm

The leading paradigm in compressed hydrides from Ashcroft is the need to break, or deter, the strong H_2 molecular bond or other molecular bonds (viz., CH_4 and NH_3), which will move the bonding band below E_F and push the antibonding bands above E_F, leaving little or no H contribution at the Fermi level. Breaking up molecules, leaving open $1s$ shell atomic hydrogen rather than molecular hydrogen, is the paradigm followed by the three first discoveries, and by nearly all of the predicted hydrides with $T_c > 100$ K. As it has been the leading concept for 60 years, little more needs to be said about this paradigm, but since this is a new field of investigation and discovery, it is important to look for other paradigms.

2. An alternative paradigm: Activating bonding states

The RTS examples introduced in Sec. V are from the anticipated class, in which hydrogen becomes atomic (no overt covalent bonding) and predominantly H $1s$ bands lie at the Fermi level and are primarily, almost overwhelmingly, responsible for high T_c. Computational explorations of ternary hydrides (discussed later) have found that at sufficiently low pressures cells with molecular H_2 or H-rich molecules provide stable structures. In such compounds, bonding and antibonding H $1s$ levels are split from the Fermi level (below and above, respectively) and H vibrations provide little or no EP coupling. It seems that a guiding principle is that atomic H dominance leads over other productive possibilities, and its coupling strength requires further attention. Yet another possibility has arisen.

Li_2MgH_{16}.—Sun *et al.* (2019) reported a calculation of T_c around 475 K at 250 GPa for Li_2MgH_{16}, which is best pictured as a lattice of MgH_{16} clathratelike units intercalated by Li. The large unit is rather stable, while the Li donor adds electrons, lends the H sites a more metallic character, and doubles the value of $N(0)$. The maximum H frequency was 2400 cm^{-1}, which is in the same range as other HTS hydrides at similar or somewhat lower pressure. As in other hydrides, T_c decreases with increasing pressure, while the frequency spectrum increases.

The distinction that makes T_c higher than in other compressed hydrides is unclear. The small mass of Li results in the overlap of its phonon projected density of states with that of H; Mg is lower and nearly separate. For $\lambda = 3.35$ in this P-T_c regime, roughly 1.75 can be ascribed to the low frequency metal atoms ($\omega < 20$ THz), with 1.60 arising from H modes extending up to 70 THz. The two H sites contribute significantly differently to the bands crossing the Fermi level (Quan and Pickett, 2022). A comparative analysis with other HTS compressed hydrides is needed to obtain insight into the origins of high T_c.

LiB_2H_8.—As another example, Gao *et al.* reported in 2021 a designed (predicted) H-rich system (Gao *et al.*, 2021) in which high T_c (though not RTS) arises in a distinctive manner. The material is one in which BH_4 units (identifiable molecules) lie in interstitial positions within a bcc potassium sublattice, comprising $KB_2H_8 = K(BH_4)_2$, with identifiable BH_4 molecules. Extrapolating from results on other ternaries, such a compound having only molecular hydrogen, should be unpromising. However, the chemistry (more specifically, the Madelung potential) is such that each molecular BH_4 radical [likely unstable in itself, lacking the extra electron that stabilizes methane (CH_4)] obtains 1/2 electron from the K ion, leaving the uppermost (least strongly bound) molecular orbital half empty. The resulting radicals are stable within the sublattice of positive K ions, and the compound is predicted to be dynamically stable.

KB_2H_8 is calculated to be metallic, but with the character of a heavily hole-doped wide-gap insulator. This leaves covalently bonded bands that are strongly coupled to B-H bond-stretch modes at the Fermi level, a close analog (An and Pickett, 2001) of MgB_2 with its $T_c = 40$ K. The calculation of Gao *et al.* gave $T_c \approx 140$ K at a modest pressure of only 12 GPa, arising from large $\lambda = 3$ but an unusually low frequency scale $\omega_{log} = 33$ meV (+100 meV is more typical of RTS hydrides, but at pressures of 150 GPa and higher). This is a three-dimensional extension of the argument that such MgB_2-like systems can be optimized to produce much higher EP-coupled superconductivity (Pickett, 2008). Further improvements in this direction seem possible.

However, with such a large hole density that covalent bonds may be unstable, LiB_2H_8 may not be a thermodynamically stable composition. This scenario played out in $Li_{1-x}BC$, where, for $x \sim 0.2$–0.3, T_c up to 75 K was inferred (Rosner, Kitaigorodsky, and Pickett, 2002). Substantial experimental effort (Fogg *et al.*, 2003) could not produce metallic transport at the target doping levels, instead obtaining distorted and disordered materials. However, Sr^{2+} doping on the K^{1+} sites, lowering the hole doping level, and broader synthesis routes may provide the pathways to desired materials (Nakamori and Orimo, 2004).

D. Increasing accessibility: Metastable structures

1. Lowering the required pressure

Of growing concern is to find, perhaps by design and discovery or perhaps by serendipity, materials that will retain their high-pressure high values of T_c to lower pressures, with the intention of finding applications. Most of the binary hydrides have been explored with computational means (Bi *et al.*, 2017; Flores-Livas *et al.*, 2020). Analysis of the results still must be done, and published results often do not provide much of the required information, including the atom-specific quantities in λ in Eq. (9). Quan, Ghosh, and Pickett (2019) initiated such an analysis but were limited to a few binary hydrides, for which their recalculations provided the data required for an analysis of the electronic properties.

Separately but equally valuable is an improved understanding of the stability, or lack thereof, of high T_c materials composition and structures. Speaking broadly, there are several examples of this scenario: a high T_c material is discovered (either computationally or experimentally) and its structure understood; pressure is lowered and T_c (and calculated λ) increases but a phonon branch is lowered; a structural phase transition occurs at a critical pressure P_{cr}; in the low-pressure phase T_c is much lower or perhaps

vanishing; and the structure of the new phase includes H-rich molecular units, including possibly H_2, without much or any atomic hydrogen. One question being addressed is: How can this process be pushed to lower P_{cr}, or even (ideally) to ambient pressure?

2. More complex hydrides and speeding searches

Since the previously discussed design and discovery, emphasis has broadened. Higher values of T_c are still of great interest; after all, applications at room temperature will require T_c around 30% higher (375–400 K), or even higher for high current density applications. Given the considerable number of binary hydrides that have been modeled and mined for high T_c (here meaning roughly $T_c > 100$ K, which is useful for applications), searches are now being extended to ternary hydrides.

The palette of ternary hydrides is much larger than that of binaries, thereby providing new candidates and new computational challenges. Thus far the emphasis has been on the more H-rich possibilities, viz., $A_iB_jH_n$ with small i and j and larger n. With atoms A and B selected from, say, the 60 most reasonable choices of elements, and with concentration n ranging up to 12, this class has on the order of 10^4–10^5 formulas, and for each of these many crystal structures are possible. Given this complexity, techniques in high-throughput computing, dataset construction, and data mining, coupled with machine learning, are being applied to the search for promising candidates, but a full search is not in sight. Background on these activities was given in the 2021 road map compilation (Boeri *et al.*, 2022). There are too many reports already on ternary hydrides with too little analysis to attempt to provide an overview. Several candidates have predicted $T_c > 100$ K; however, explorations of the generalized convex hull to find the most stable stoichiometries have been limited.

3. Exploring higher pressures

While discussion of advancing high-pressure techniques is well beyond the scope of this Colloquium, note that experimental extensions to achieve higher pressures more readily, and to adapt measurement techniques to obtain more general data on the samples, are continually pursued in the high-pressure laboratories that have contributed to high T_c hydrides at high pressure.

VII. REGULARITIES IN COMPRESSED HYDRIDES

While this Colloquium is not intended as a topical review of compressed hydrides, questions have been raised and, in some cases, addressed concerning the properties that provide a close approach to room temperature superconductivity. Several features that appear to be important clues, i.e., to have some generality, have been identified.

• Fundamental questions are: What structure types of compressed hydrides are favored, and in what pressure ranges? Some guidelines seem to have arisen. In the lower pressure range, hydrogen molecule phases arise and are poor superconductors or, often not reported, insulators. At higher pressure (say, 150–300 GPa), atomic hydrogen structures are frequently favored, with H-caged metal structures (such as clathrate) being common. At still higher pressures (with fewer published examples) less common structures are predicted; for example, one has several layers of hydrogen followed by a few layers of metal, suggestive of incipient phase separation. This area is a complex one, and the reviews and overviews mentioned later should be consulted.

• An overriding question remains open to clarification: What properties enable room temperature superconductivity? It is not large λ *per se*; $\lambda \approx 2$–3 is similar to that in Pb-Th-Bi alloys, with their $T_c \approx 10$ K. These low T_c materials have soft phonons, due to heavy masses and nondescript s-p bonding. Compressed hydrides have frequency scales up to 150–200 meV (1750–2300 K) compared to those heavy atoms with frequency scales of 50–75 K. The enabling feature is, as Ashcroft foretold, producing H-derived modes at high frequency while retaining strong coupling to Fermi surface carriers. This is, however, more of an observation than an answer.

• *Strong coupling*.—Barring innovations, larger λ should not be the overriding aspiration. There are numerous cases, including the previously mentioned compressed hydrides, where increasing λ increases T_c but rapidly encounters soft phonons and lattice instability. λ is an unreliable descriptor for a high T_c search. A clue is that η/M, independent of frequencies, is much better (Allen and Dynes, 1975; Quan, Ghosh, and Pickett, 2019). Since higher frequency scales will likely require ever higher pressures, the alternative seems to be pushing strong coupling to the high frequency region. In compressed hydrides "bond-stretch" modes seem not to be a dominant consideration. Generally H–H "bonding" is not a clear feature; H-metal bonding is more often a topic of consideration.

• Semenok *et al.* (2020) and Belli *et al.* (2021) observed that atoms in columns I, II, and III provide, with occasional exceptions, the binary hydrides with high T_c. These atoms have low electronegativity, readily donating electrons to the H sublattice(s). The resulting negatively charged H atoms (versus neutral, half-filled entities such as the H_2 molecule) promote breaking of H bonds and production of metallic ground states. This factor might also be related to the retention of strong coupling to high energy vibrations.

• Is a higher concentration of H the key? Indications are that a large fraction of H states at the Fermi surface, i.e., reflected in a large ratio $N_H(0)/N(0)$, is not a clear determining factor, or is at least not essential. This is a straightforward band structure quantity and cannot be estimated before the band calculation is done, because band structure effects cause the structure in $N(\varepsilon)$. As an example of this item, SH_3 is somewhat exceptional, with a strong van Hove peak at the Fermi level. Ghosh, Quan, and Pickett (2019), Pickard, Errea, and Eremets (2020), and Flores-Livas *et al.* (2020) highlighted the $N(0)$ factor in compressed hydrides.

• Producing "atomic hydrogen," as opposed to molecular-bonded hydrogen, has been the overriding objective, and thus far the productive one. Pressure will eventually decompose hydrogen-rich molecules, but other methods (viz., doping) should be kept in mind. Doping holes into bonding states may be promising (Gao *et al.*, 2021), but too much doping will make a stable phase prone to structural instabilities.

• *Lattice instabilities*.—In several cases of high T_c hydrides, it has been found that within a given phase T_c decreases with increasing pressure. Conversely, T_c increases as pressure is decreased, λ increases, and the modes giving the increase in λ are renormalized to lower frequency and then become dynamically unstable. For the five systems illustrating this self-limiting process in Fig. 10(d), there is an indication of a phase boundary for binary hydrides in the ω_2-T_c plane.

• The lattice stiffness $\kappa_H = M_H \omega_{2,H}^2$ increases with pressure. However, strong coupling is far from uniform throughout the H-derived optic modes. Pressure does increase the frequency scale, but appearing squared in the denominator it decreases λ. This trade-off has long been a persistent issue in the pursuit of higher T_c superconductivity. More focus needs to be aimed at increasing η_H.

• The scattering efficacy of the vibrating H atom $\mathcal{I}_H^2$ increases with pressure, according to current information (Papaconstantopoulos *et al.*, 2015; Quan, Ghosh, and Pickett, 2019). The origin of this simple fact is unclear, but the theoretical and computational means to understand it is available within DFT codes (but with proper extraction and analysis required).

• For the small set of examples that has been studied, $\mathcal{I}_H^2$ varies from one to another over the pressure range of interest by a factor of 3, and η by a factor of 2, (Quan, Ghosh, and Pickett, 2019); see Fig. 12. This difference can be partially attributed to broadening of the largely H bandwidth with increasing pressure, hence tending to decrease $N_H(0)$. Again the origin is unclear, but there is a detailed computational theory for analyzing this fact in detail.

A careful study of the previously listed "regularities" will reveal repetition and apparent inconsistencies and contradictions. For example, strong coupling at high frequency is most important, but also $\eta = N(0)\mathcal{I}^2$ (which is independent of frequency) is what matters most at strong coupling. Such viewpoints must be confronted in the quest for higher T_c at lower pressure. In addition, nearly universally high T_c has been couched separately in terms of λ and one characteristic phonon frequency, viz., ω_{log}. This approach my be misguided (i.e., not the most profitable) for progress. It has been noted that, for the five previously mentioned compressed hydrides, the simple relation $T_c \propto A$, where A is the area under $\alpha^2 F$, works well despite its simplicity (Quan, Ghosh, and Pickett, 2019). Improvements in the T_c equation and in understanding by a generalization to another one to three more characteristics obtained from $\alpha^2 F$.

VIII. CONCLUSIONS

A number of overviews (Boeri and Bachelet, 2019; Pickett and Eremets, 2019; Pickard, Errea, and Eremets, 2020; Shimizu, 2020) and more extensive collections (Bi *et al.*, 2017; Zurek and Bi, 2019; Flores-Livas *et al.*, 2020; Semenok *et al.*, 2020; Boeri *et al.*, 2022; Hilleke, Bi, and Zurek, 2022; Hilleke and Zurek, 2022) on predictions of hydride superconductivity are available. The achievement of near room temperature superconductivity has stimulated extensions of high-pressure techniques and the enabling of additional measurements, in step with improved analysis and interpretation of data (Hemley *et al.*, 2019; Guan, Hemley, and Viswanathan, 2021).

The first point of this perspective was provided in Secs. II and III, which summarized the sequence of theoretical and algorithmic advances, followed by numerical implementation, that have produced an accurate, material-specific theory of EP superconducting T_c, as well as several superconducting properties not discussed here, stemming mostly from the complex superconducting gap $\Delta(\omega, T)$. The three initial advances predicted by the theory and then confirmed by experiment were discussed in Sec. V:

• SH_3, 200 K at 100 GPa.
• LaH_{10}, 260 K at 200 GPa.
• YH_9, 240–260 K at around 250 GPa.

This Colloquium provides an overview of the theory-driven forces behind the design and discovery of room temperature superconductivity. The experimental effort on hydrides has been impressive as well. Room temperature superconductivity was a much discussed but distant goal in the 1970s, but expectations faded after 13 years with no increase in T_c. The discovery of high T_c cuprates revived the dream to some extent, but the focus of research soon reverted to an intense study of the properties and mechanisms (versus the magnitude of T_c) of superconducting quantum materials, a topic that remains a leading paradigm of condensed matter physics that is being broadened to other classes, properties, and applications. In terms of temperature, HTS has been superseded only by compressed hydrides—the long-sought room temperature superconductors.

REFERENCES

Akashi, R., M. Kawamura, S. Tsuneyuki, Y. Nomura, and R. Arita, 2015, "First-principles study of the pressure and crystal structure dependencies of the superconducting transition temperature of compressed sulfur hydrides," Phys. Rev. B **91**, 060511(R).

Allen, P. B., 1973, "Repulsive effect of low frequency phonons on superconductivity," Solid State Commun. **12**, 379.

Allen, P. B., 1974, "Effect of soft phonons on superconductivity: A re-evaluation and a positive case for Nb_3Sn," Solid State Commun. **14**, 937.

Allen, P. B., 1979, "Theory of superconducting transition temperature, pair susceptibility, and coherence length," in *Lecture Notes in Physics, XVI Karpacz Winter School of Theoretical Physics* (Springer-Verlag, Berlin).

Allen, P. B., 1980, "Phonons and the superconducting transition temperature," in *Dynamical Properties of Solids*, edited by G. K. Horton and A. A. Maradudin (North-Holland, Amsterdam).

Allen, P. B., M. L. Cohen, and D. R. Penn, 1988, "Total dielectric function: Algebraic sign, electron-lattice response, and superconductivity," Phys. Rev. B **38**, 2513.

Allen, P. B., and R. C. Dynes, 1975, "Transition temperature of strong-coupled superconductors reanalyzed," Phys. Rev. B **12**, 905.

Allen, P. B., and B. Mitrović, 1983, "Theory of superconducting T_c," in *Solid State Physics*, Vol. 37, edited by H. Ehrenreich, F. Seitz, and D. Turnbull (Academic, New York), p. 1.

An, J. M., and W. E. Pickett, 2001, "Superconductivity of MgB_2: Covalent Bonds Driven Metallic," Phys. Rev. Lett. **86**, 4366.

Ashcroft, N. W., 1968, "Metallic Hydrogen: A High-Temperature Superconductor?," Phys. Rev. Lett. **21**, 1748.

Ashcroft, N. W., 2004, "Hydrogen Dominant Metallic Alloys: High Temperature Superconductors?," Phys. Rev. Lett. **92**, 187002.

Bardeen, J., L. N. Cooper, and J. R. Schrieffer, 1957, "Theory of superconductivity," Phys. Rev. Res. **108**, 1175.

Bauer, J., J. E. Han, and O. Gunnarsson, 2011, "Quantitative reliability study of the Migdal-Eliashberg theory for strong electron-phonon coupling in superconductors," Phys. Rev. B **84**, 184531.

Belli, F., T. Novoa, J. Contreras-Garcia, and Y. Errea, 2021, "Strong correlation between electron bonding network and critical temperature in hydrogen-based superconductors," Nat. Commun. **12**, 5381.

Bergerhoff, G., R. Hundt, R. Sievers, and I. D. Brown, 1983, "The inorganic crystal structure data base," J. Chem. Inf. Comput. Sci. **23**, 66.

Bergmann, G., and D. Rainer, 1973, "The sensitivity of the transition temperature to changes in $\alpha^2 F(\omega)$," Z. Phys. **263**, 59.

Bi, T., N. Zarifi, T. Terpstra, and E. Zurek, 2017, "The search for superconductivity in high pressure hydrides," in *Elsevier Reference Module in Chemistry, Molecular Sciences and Chemical Engineering*, edited by J. Reedijk (Elsevier, Waltham, MA).

Boeri, L., and G. B. Bachelet, 2019, "Viewpoint: The road to room-temperature conventional superconductivity," J. Phys. Condens. Matter **31**, 234002.

Boeri, L., *et al.*, 2022, "The 2021 room-temperature superconductivity roadmap," J. Phys. Condens. Matter **34**, 183002.

Chubukov, A. V., A. Abanov, I. Esterlis, and S. A. Kivelson, 2020, "Eliashberg theory of phonon-mediated superconductivity—When it is valid and how it breaks down," Ann. Phys. (Amsterdam) **417**, 168190.

Cockayne, E., 2005, "Generation of lattice Wannier functions via maximum localization," Phys. Rev. B **71**, 094302.

Curtarolo, S., *et al.*, 2012, "AFLOW: An automatic framework for high-throughput materials discovery," Comput. Mater. Sci. **58**, 218.

Drozdov, A. P., M. I. Eremets, and I. A. Troyan, 2014, "Conventional superconductivity at 190 K at high pressures," arXiv:1412.0460.

Drozdov, A. P., M. I. Eremets, I. A. Troyan, V. Ksenofontovand, and S. I. Shylin, 2015, "Conventional superconductivity at 203 kelvin at high pressures in the sulphur hydride system," Nature (London) **525**, 73.

Drozdov, A. P., V. S. Minkov, S. P. Besedin, M. A. Kuzovnikov, D. A. Knyazev, and M. I. Eremets, 2018, "Superconductivity at 215 K in lanthanum hydride at high pressures," arXiv:1808.07039.

Drozdov, A. P., *et al.*, 2019, "Superconductivity at 250 K in lanthanum hydride under high pressures," Nature (London) **569**, 528.

Duan, D., Y. Liu, F. Tian, D. Li, X. Huang, Z. Zhao, H. Yu, B. Liu, W. Tian, and T. Cui, 2014, "Pressure-induced metalization of dense $(H_2S)_2H_2$ with high-T_c superconductivity," Sci. Rep. **4**, 6968.

Einaga, M., M. Sakata, T. Ishikawa, K. Shimizu, M. Eremets, A. Drozdov, I. Troyan, N. Hirao, and Y. Ohishi, 2016, "Crystal structure of 200 K superconducting phase of sulfur hydride system," Nat. Phys. **12**, 835.

Eliashberg, G. M., 1960, "Interactions between electrons and lattice vibrations in a superconductor," Sov. Phys. JETP **11**, 696.

Eliashberg, G. M., 1961, "Temperature Green's function for electrons in a superconductor," Sov. Phys. JETP **12**, 1000.

Emery, V. J., and S. A. Kivelson, 1995, "Importance of phase fluctuations in superconductors with small superfluid density," Nature (London) **374**, 434.

Eremets, M., *et al.*, 2022, "High-temperature superconductivity in hydrides: Experimental evidence and details," J. Supercond. Novel Magn. **35**, 965.

Errea, I., M. Calandra, C. J. Pickard, J. Nelson, R. J. Needs, Y. Li, H. Liu, Y. Zhang, Y. Ma, and F. Mauri, 2015, "High-Pressure Hydrogen Sulfide from First Principles: A Strongly Anharmonic Phonon-Mediated Superconductor," Phys. Rev. Lett. **114**, 157004.

Errea, I., *et al.*, 2020, "Quantum crystal structure in the 250-kelvin superconducting lanthanum hydride," Nature (London) **578**, 66.

Flores-Livas, J. A., L. Boeri, A. Sanna, G. Profeta, R. Arita, and M. Eremets, 2020, "A perspective on conventional high-temperature superconductors at high pressure: Methods and materials," Phys. Rep. **856**, 1.

Fogg, A. M., J. B. Claridge, G. R. Darling, and M. J. Rosseinsky, 2003, "Synthesis and characterization of Li_xBC: Hole doping does not induce superconductivity," Chem. Commun. (Cambridge) **9**, 1348.

Gao, L., Xue, Y. Y., F. Chen, Q. Xiong, R. L. Meng, D. Ramirez, C. W. Chu, J. H. Eggert, and H. K. Mao, 1994, "Superconductivity up to 164 K in $HgBa_2Ca_{m-1}$ $Cu_mO_{2+\delta}$ ($m = 1$, 2, and 3) under quasihydrostatic pressures," Phys. Rev. B **50**, 4260.

Gao, M., X.-W. Yan, Z.-Y. Lu, and T. Xiang, 2021, "Phonon-mediated high-temperature superconductivity in the ternary borocarbide KB_2H_8 under pressure near 12 GPa," Phys. Rev. B **104**, L100504.

Gaspari, G. D., and B. L. Gyorffy, 1972, "Electron-Phonon Interactions, d Resonances, and Superconductivity in Transition Metals," Phys. Rev. Lett. **28**, 801.

Ge, Y., F. Zhang, and R. J. Hemley, 2021, "Room-temperature superconductivity in boron- and nitrogen-doped lanthanum superhydride," Phys. Rev. B **104**, 214505.

Geballe, Z. M., H. Liu, A. K. Mishra, M. Ahart, M. Somayazulu, Y. Meng, M. Baldini, and R. J. Hemley, 2018, "Synthesis and stability of lanthanum superhydrides," Angew. Chem., Int. Ed. Engl. **57**, 688.

Ghosh, S. S., Y. Quan, and W. E. Pickett, 2019, "Strong particle-hole asymmetry in a 200 kelvin superconductor," Phys. Rev. B **100**, 094521.

Ginzburg, V. L., and L. D. Landau, 1950, "On the theory of superconductivity," Zh. Eksp. Teor. Fiz. **20**, 1064; English translation in *Collected Papers of L. D. Landau*, translated by D. Ter Haar (Pergamon Press, Oxford, 1965), p. 546.

Giustino, F., 2014, *Materials Modeling Using Density Functional Theory: Properties and Predictions* (Oxford University Press, Oxford).

Giustino, F., 2017, "Electron-phonon interactions from first principles," Rev. Mod. Phys. **89**, 015003.

Glass, C. W., A. R. Oganov, and N. Hansen, 2006, "USPEX— Evolutionary crystal structure prediction," Comput. Phys. Commun. **175**, 713.

Gor'kov, L. P., 1958, "On the energy spectrum of superconductors," Sov. Phys. JETP **7**, 158.

Guan, P.-W., R. J. Hemley, and V. Viswanathan, 2021, "Combining pressure and electrochemistry to synthesize superhydrides," Proc. Natl. Acad. Sci. U.S.A. **118**, e2110470118.

Heil, C., S. di Cataldo, G. B. Bachelet, and L. Boeri, 2019, "Superconductivity in sodalite-like yttrium hydride clathrates," Phys. Rev. B **99**, 220502.

Hemley, R. J., M. Ahart, H. Liu, and M. Somayazulu, 2019, "Road to room-temperature superconductivity: T_c above 260 K in lanthanum superhydride under pressure," arXiv:1906.03462.

Hilleke, K. P., T. Bi, and E. Zurek, 2022, "Materials under high pressure: A chemical perspective," Appl. Phys. A **128**, 441.

Hilleke, K. P., and E. Zurek, 2022, "Tuning chemical precompression: Theoretical design and crystal chemistry of novel hydrides in the quest for warm and light superconductivity at ambient pressures," J. Appl. Phys. **131**, 070901.

Hohenberg, P., and W. Kohn, 1964, "Inhomogeneous electron gas," Phys. Rev. **136**, B864.

Huang, K., *et al.*, 2019, "High-temperature superconductivity in sulfur hydride evidenced by alternating-current magnetic susceptibility," Natl. Sci. Rev. **6**, 713.

Hutcheon, M. J., A. M. Shipley, and R. J. Needs, 2020, "Predicting novel superconducting hydrides using machine learning approaches," Phys. Rev. B **101**, 144505.

Kohn, W., and L. J. Sham, 1965, "Inhomogeneous electron gas," Phys. Rev. **140**, A1133.

Kong, P. P., *et al.*, 2019, "Superconductivity up to 243 K in yttrium hydrides under high pressure," arXiv:1909.10482.

Kong, P. P., *et al.*, 2021, "Superconductivity up to 243 K in the yttrium-hydrogen system under high pressure," Nat. Commun. **12**, 5075.

Li, Y., J. Hao, H. Liu, Y. Li, and Y. Ma, 2014, "The metalization and superconductivity of dense hydrogen sulfide," J. Chem. Phys. **140**, 174712.

Li, Y., J. Hao, H. Liu, J. S. Tse, Y. Wang, and Y. Ma, 2015, "Pressure-stabilized superconductive yttrium hydrides," Sci. Rep. **5**, 9948.

Liu, H., I. I. Naumov, Z. M. Geballe, M. Somayazulu, J. S. Tse, and R. J. Hemley, 2018, "Dynamics and superconductivity in compressed lanthanum superhydride," Phys. Rev. B **98**, 100102(R).

Liu, H., I. I. Naumov, R. Hoffman, N. W. Ashcroft, and R. J. Hemley, 2017, "Potential high T_c superconducting lanthanum and yttrium hydrides at high pressure," Proc. Natl. Acad. Sci. U.S.A. **114**, 6990.

Liu, L., C. Wang, S. Yi, K. W. Kim, J. Kim, and J.-H. Cho, 2019, "Origin of high-temperature superconductivity in compressed LaH_{10}," Phys. Rev. B **99**, 140501.

Lonie, D. C., and E. Zurek, 2011, "XtalOpt: An open-source evolutionary algorithm for crystal structure prediction," Comput. Phys. Commun. **182**, 372–387.

Lüders, M., M. A. L. Marques, N. N. Lathiotakis, J. A. Flores-Livas, G. Profeta, L. Fast, A. Continenza, S. Massidda, and E. K. U. Gross, 2005, "*Ab initio* theory of superconductivity. I. Density functional formalism and approximate functionals," Phys. Rev. B **72**, 024545.

Margine, E. R., and F. Giustino, 2013, "Anisotropic Midgal-Eliashberg theory using Wannier functions," Phys. Rev. B **87**, 024505.

Marques, M. A. L., M. Lüders, N. N. Lathiotakis, J. A. Flores-Livas, G. Profetaand L. Fast, A. Continenza, S. Massidda, and E. K. U. Gross, 2005, "*Ab initio* theory of superconductivity. II. Application to elemental metals," Phys. Rev. B **72**, 024546.

Matthias, B. T., 1972, "Higher temperatures and instabilities," AIP Conf. Proc. **4**, 367.

McMahon, J. M., and D. Ceperley, 2011, "High-temperature superconductivity in atomic metallic hydrogen," Phys. Rev. B **84**, 144515.

McMillan, W. L., 1968, "Transition temperature of strong-coupled superconductors," Phys. Rev. **167**, 331.

Migdal, A. B., 1958, "Interactions between electrons and lattice vibrations in a normal metal," Sov. Phys. JETP **7**, 1438.

Minkov, V. S., S. Bud'ko, F. Balakirev, V. Prakapenka, S. Chariton, R. J. Husband, H. P. Liermann, and M. Eremets, 2022, "Magnetic field screening in hydrogen-rich high-temperature superconductors," Nat. Commun. **13**, 3194.

Minkov, V. S., V. Ksenofontov, S. L. Budko, E. F. Talantsev, and M. I. Eremets, 2022, "Trapped magnetic flux in hydrogen-rich high-temperature superconductors," arXiv:2206.14108.

Mostofia, A. A., J. R. Yates, Y.-S. Lee, I. Souza, D. Vanderbilt, and N. Marzari, 2008, "Wannier90: A tool for obtaining maximally-localised Wannier functions," Comput. Phys. Commun. **178**, 685.

Nakamori, Y., and S.-I. Orimo, 2004, "Synthesis and characterization of single phase Li_xBC ($x = 0.5$ and 1.0), using Li hydride as a starting material," J. Alloys Compd. **370**, L7.

Oganov, A. R., 2010, Ed., *Modern Methods of Crystal Structure Prediction* (Wiley-VCH, Berlin).

Papaconstantopoulos, D. A., B. M. Klein, M. J. Mehl, and W. E. Pickett, 2015, "Cubic H_3S around 200 GPa: An atomic hydrogen superconductor stabilized by sulfur," Phys. Rev. B **91**, 184511.

Peng, F., Y. Sun, C. J. Pickard, R. J. Needs, Q. Wu, and Y. Ma, 2017, "Hydrogen Clathrate Structures in Rare Earth Hydrides At High Pressures: Possible Route to Room-Temperature Superconductivity," Phys. Rev. Lett. **119**, 107001.

Pickard, C. J., I. Errea, and M. I. Eremets, 2020, "Superconducting hydrides under pressure," Annu. Rev. Condens. Matter Phys. **11**, 57.

Pickard, C. J., and R. J. Needs, 2011, "*Ab initio* random structure searching," J. Phys. Condens. Matter **23**, 053201.

Pickett, W. E., 1979, "The generalized pseudoatom potential in solids: Relation to screening and lattice dynamics," J. Phys. C **12**, 1491.

Pickett, W. E., 2008, "The next breakthrough in phonon-mediated superconductivity," Physica (Amsterdam) **468C**, 126.

Pickett, W. E., and M. Eremets, 2019, "The quest for room-temperature superconductivity in hydrides," Phys. Today **72**, No. 5, 52.

Quan, Y., S. S. Ghosh, and W. E. Pickett, 2019, "Compressed hydrides as metallic hydrogen superconductors," Phys. Rev. B **100**, 184505.

Quan, Y., and W. E. Pickett, 2022 (unpublished).

Rabe, K. M., and U. V. Wagmare, 1995, "Localized basis for effective lattice Hamiltonians: Lattice Wannier functions," Phys. Rev. B **52**, 13236.

Rosner, H., A. Kitaigorodsky, and W. E. Pickett, 2002, "Prediction of High T_c Superconductivity in Hole-Doped LiBC, Phys. Rev. Lett. **88**, 127001.

Sanna, A., 2017, "Introduction to superconducting density functional theory," in *The Physics of Correlated Insulators, Metals, and Superconductors*, edited by E. Pavarini, E. Koch, R. Scalettar, and R. M. Martin (Forschungszentrum, Jülich, Germany).

Sanna, A., C. Pellegrini, and E. K. U. Gross, 2020, "Combining Eliashberg Theory with Density Functional Theory for the Accurate Prediction of Superconducting Transition Temperatures and Gap Functions," Phys. Rev. Lett. **125**, 057001.

Scalapino, D. J., 1969, "The electron-phonon interaction and strong-coupling superconductivity," in *Superconductivity*, edited by R. D. Parks (Marcel Dekker, New York), p. 561.

Scalapino, D. J., J. R. Schrieffer, and J. W. Wilkins, 1966, "Strong-coupling superconductivity I," Phys. Rev. **148**, 263.

Schrodi, F., P. M. Oppeneer, and A. Aperis, 2020, "Full-bandwidth Eliashberg theory of superconductivity beyond Migdal's approximation," Phys. Rev. B **102**, 024503.

Semenok, D. V., I. A. Kruglov, I. A. Savkin, A. G. Kvanhnin, and A. R. Oganov, 2020, "On distribution of superconductivity in metal hydrides," Curr. Opin. Solid State Mater. Sci. **24**, 100808.

Semenok, D. V., *et al.*, 2021, "Superconductivity at 253 K in lanthanum-yttrium ternary hydrides," Mater. Today **48**, 18.

Shimizu, K., 2020, "Investigation of superconductivity in hydrogen-rich systems," J. Phys. Soc. Jpn. **89**, 051005.

Snider, E., N. Dasenbrock-Gammon, R. McBride, X. Wang, N. Meyers, K. V. Lawler, E. Zurek, A. Salamat, and R. P. Dias, 2021, "Synthesis of Yttrium Superhydride Superconductor with a Transition Temperature up to 262 K by Catalytic Hydrogenation at High Pressures," Phys. Rev. Lett. **126**, 117003.

Somayazulu, M., M. Ahart, A. K. Mishra, Z. M. Geballe, M. Baldini, Y. Meng, V. V. Struzhkin, and R. J. Hemley, 2019, "Evidence for Superconductivity above 260 K in Lanthanum Superhydride at Megabar Pressures," Phys. Rev. Lett. **122**, 027001.

Stanev, V., C. Oses, A. G. Kusne, E. Rodriguez, J. Paglione, S. Curtarolo, and I. Takeuchi, 2018, "Machine learning modeling of superconducting critical temperature," npj Comput. Mater. **4**, 29.

Sun, Y., J. Lv, Y. Xie, H. Liu, and Y. Ma, 2019, "Route to a Superconducting Phase above Room Temperature in Electron-Doped Hydride Compounds under High Pressure," Phys. Rev. Lett. **123**, 097001.

Troyan, I. A., *et al.*, 2021, "Anomalous high-temperature superconductivity in YH_6," Adv. Mater. **33**, 2006832.

Yang, C. N., 1962, "Concept of off-diagonal long-range order and the quantum phases of liquid He and of superconductors," Rev. Mod. Phys. **34**, 694.

Yang, Y., J. Lv, L. Zhu, and Y. Ma, 2012, "CALYPSO: A method for crystal structure prediction," Comput. Phys. Commun. **183**, 2063.

Zurek, E., and T. Bi, 2019, "High temperature superconductivity in alkaline and rare earth polyhydrides at high pressures: A theoretical perspective," J. Chem. Phys. **150**, 050901.

See Supplemental Material at http://link.aps.org/supplemental/10.1103/RevModPhys.95.021001 for an mp4 file showing a dynamic simulation of the SH_3 lattice.